

**This is a self-archived version of an original article. This version may differ from the original in pagination and typographic details.**

**Author(s):** Joukainen, Henna; Ruotsalainen, Panu; Sarén, Jan; Srivastava, Praveen C.; Patel, Deepak; Julin, Rauno; Auranen, Kalle; Ge, Zhuang; Grahn, Tuomas; Greenlees, Paul; Illana, Andres; Jutila, Henri; Leino, Matti; Louko, Jussi; Luoma, Minna; Ojala, Joonas; Pakarinen, Janne; Rahkila, Panu; Sandzelius, Mikael; Tann, Holly; Uusitalo, Juha; Zimba, George L.

**Title:**  $\gamma$  -Ray spectroscopy above the 9+ isomeric state in the N = Z nucleus 66As

**Year:** 2024

**Version:** Published version

**Copyright:** © The Author(s) 2024

**Rights:** CC BY 4.0


**Rights url:** <https://creativecommons.org/licenses/by/4.0/>

**Please cite the original version:**

Joukainen, H., Ruotsalainen, P., Sarén, J., Srivastava, P. C., Patel, D., Julin, R., Auranen, K., Ge, Z., Grahn, T., Greenlees, P., Illana, A., Jutila, H., Leino, M., Louko, J., Luoma, M., Ojala, J., Pakarinen, J., Rahkila, P., Sandzelius, M., . . . Zimba, G. L. (2024).  $\gamma$  -Ray spectroscopy above the 9+ isomeric state in the N = Z nucleus 66As. *European Physical Journal A*, 60, Article 241.  
<https://doi.org/10.1140/epja/s10050-024-01458-5>



# $\gamma$ -Ray spectroscopy above the $9^+$ isomeric state in the $N = Z$ nucleus $^{66}\text{As}$

Henna Joukainen<sup>1,a</sup> , Panu Ruotsalainen<sup>1,b</sup>, Jan Sarén<sup>1,c</sup>, Praveen C. Srivastava<sup>2</sup>, Deepak Patel<sup>2</sup>, Rauno Julin<sup>1</sup>, Kalle Auranen<sup>1</sup>, Zhuang Ge<sup>1</sup>, Tuomas Grahn<sup>1</sup>, Paul Greenlees<sup>1</sup>, Andres Illana<sup>1,3</sup>, Henri Jutila<sup>1</sup>, Matti Leino<sup>1</sup>, Jussi Louko<sup>1</sup>, Minna Luoma<sup>1</sup>, Joonas Ojala<sup>1</sup>, Janne Pakarinen<sup>1</sup>, Panu Rahkila<sup>1</sup>, Mikael Sandzelius<sup>1</sup>, Holly Tann<sup>1</sup>, Juha Uusitalo<sup>1</sup>, George L. Zimba<sup>1,4</sup>

<sup>1</sup> Accelerator Laboratory, Department of Physics, University of Jyväskylä, 40014 Jyväskylä, Finland

<sup>2</sup> Department of Physics, Indian Institute of Technology Roorkee, Roorkee 247667, India

<sup>3</sup> Present address: Grupo de Física Nuclear & CEI Moncloa, IPARCOS, Universidad Complutense de Madrid, 28040 Madrid, Spain

<sup>4</sup> Present address: Facility for Rare Isotope Beams, Michigan State University, 640 South Shaw Lane, East Lansing, MI 48824, USA

Received: 12 June 2024 / Accepted: 18 November 2024

© The Author(s) 2024

Communicated by Robert Janssens

**Abstract** Excited states above the  $9^+$  isomer in the odd-odd  $N = Z$  nucleus  $^{66}\text{As}$  were studied by employing the  $^{40}\text{Ca}(^{28}\text{Si}, \text{pn})$  fusion-evaporation reaction at the Accelerator Laboratory of the University of Jyväskylä, Finland. A key method in this study was the use of conversion electrons emitted in the de-excitation of the isomeric state in  $^{66}\text{As}$  as a tag for prompt  $\gamma$  rays. Several new states have been added to the  $^{66}\text{As}$  level scheme, which was extended up to a tentative spin of  $23\hbar$ . The previously reported even-spin yrast band has been reassigned to have odd spin values. The odd-spin states above the  $9^+$  isomer are compared with shell-model calculations using the *jj44b* and *JUN45* interactions. Additionally, the recoil- $\beta$  tagging efficiency of the recently developed scintillator detector named *Tuik*e has been determined experimentally for the first time.

## 1 Introduction

The neutron-neutron and proton-proton pairing correlations are known to be the dominant mode in nearly all atomic nuclei. However, in  $N = Z$  nuclei, the proton-neutron (pn) pairing correlations are expected to be enhanced due to neutrons and protons occupying the same single-particle orbitals. Therefore, these nuclei provide the best testing ground to investigate the relative strengths of the pn pairing interaction in the isoscalar ( $T = 0$ ) and isovector ( $T = 1$ ) channels.

This topic has been intensively studied both theoretically and experimentally over the past few decades. A rather comprehensive review on the proton-neutron pairing is provided in Ref. [1]. In particular, the role of the isoscalar  $T = 0$ , pn pairing is still somewhat ambiguous since it is not clear how this pairing mode exhibits itself in observations. One of the fingerprints for the enhanced isoscalar correlations has been thought to be the delayed (or missing) rotational alignments observed in many  $N = Z$  systems (see e.g., Ref. [2]). Another example of enhanced  $T = 0$ , isoscalar pn correlations was proposed by Cederwall et al., in Ref. [3], where the experimentally observed yrast cascade in  $^{92}\text{Pd}$  was interpreted to result from a spin-aligned phase of isoscalar pairs of  $1g_{9/2}$  proton and neutron holes. While the observed delayed rotational alignments in  $N = Z$  nuclei and the spin-aligned coupling scheme suggested for  $^{92}\text{Pd}$  have also been explained without incorporating a strong isoscalar pn pairing interaction (see Ref. [1] and references therein), the isoscalar pn pairing can still be viewed to coexist with isovector pairing correlations in  $N = Z$  nuclei. An example of this can be found from  $^{62}\text{Ga}$ , where the  $9^+ - 17^+$  cascade has been interpreted to result from a coupling of the  $^{60}\text{Zn}$  ground-state band to an isoscalar proton-neutron pair in the  $1g_{9/2}$  orbital [4–6]. Indeed, the  $0^+ - 8^+$  ground-state band in  $^{60}\text{Zn}$  shows marked similarity with the  $9^+ - 17^+$  cascade in  $^{62}\text{Ga}$  in terms of the transition energies, in addition to the observed backbending and band termination. In analogy to this interpretation, the band based on the  $9^+$  isomer in  $^{66}\text{As}$  can be viewed to result from a coupling of the spin-aligned  $1g_{9/2}$  proton-neutron pair to the ground-state band of the triaxial nucleus  $^{64}\text{Ge}$ . It has been actually predicted in Ref. [7]

<sup>a</sup> e-mail: [henna.m.joukainen@jyu.fi](mailto:henna.m.joukainen@jyu.fi) (corresponding author)

<sup>b</sup> e-mail: [panu.ruotsalainen@jyu.fi](mailto:panu.ruotsalainen@jyu.fi)

<sup>c</sup> e-mail: [jan.saren@jyu.fi](mailto:jan.saren@jyu.fi)

that such a coupling introduces a sudden change in the triaxial rotation axis evidenced by (yet to be measured) small spectroscopic quadrupole moments in  $^{64}\text{Ge}$  and large spectroscopic quadrupole moments in  $^{66}\text{As}$ . In the present work, we guide the way to investigate this scenario in future studies by reporting results on the structure above the high-spin  $9^+$  isomer in the odd-odd,  $N = Z$  nucleus  $^{66}\text{As}$ .

The experimental studies of  $N = Z$  nuclei between the doubly-magic  $^{56}\text{Ni}$  and  $^{100}\text{Sn}$  are extremely challenging. This is reflected in the often sparse amount of available experimental data. As  $A$  increases, the  $N = Z$  line deviates rapidly from the valley of stability and approaches the proton-drip line, which signifies the limit where the nuclei become unbound. Spectroscopic studies of nuclei located close to this region are challenging due to the modest production cross sections compared to other open reaction channels. For the last few decades, the Recoil-Decay Tagging (RDT) technique has served as the method of choice for in-beam studies of nuclei near the proton-drip line (see, e.g., Refs. [8–14]). In RDT, a characteristic decay mode of a nucleus is used as a means to separate and identify the reaction products of interest among the plethora of data. Traditionally, a decay with a characteristic decay energy, i.e., an  $\alpha$  or proton decay, or an isomeric  $\gamma$ -ray transition, has been utilised as a tag. More recently,  $\beta$  decay, regardless of its continuous energy spectrum, has been shown to be usable in cases where the  $\beta$ -decay end-point energies are sufficiently high (up to  $\sim 10$  MeV) and lifetimes short ( $t_{1/2} < 100$  ms) [15–18].

In this study, we have adopted a method even more rarely used in this mass region and correlated reaction products with internal conversion electrons resulting from decays of an isomeric state, which in turn enabled an unambiguous identification of excited states above the isomer. Such correlations are not trivial for two reasons: firstly, the conversion electron energy is typically 2–3 orders of magnitude lower in comparison to the recoil energy, and secondly, the time difference between the recoil implantation and conversion electron can be extremely short. These factors impose certain requirements for the data acquisition system, i.e., the capability to trigger on small amplitude signals and separate signals occurring closely in time.

The focus of this study is the odd-odd  $N = Z$  nucleus  $^{66}\text{As}$ , where two isomeric states have been observed, reported first by Grzywacz et al. [19]. A few years later, the existence of both isomers was confirmed in a separate experiment [20], where corrected half-lives were reported and spin-parities were assigned, resulting in  $1.1(1)$   $\mu\text{s}$  and  $5^+$  for the isomer lying at 1356.7 keV and  $8.2(5)$   $\mu\text{s}$  and  $9^+$  for the one lying higher at 3023.9 keV. Additionally, six new states were added to the level scheme in Ref. [20], all placed above the  $9^+$  isomer. The most recent experimental study on  $^{66}\text{As}$  by Ruotsalainen et al. [21] again confirms the existence of the two isomeric states and their characteristics from the earlier

**Table 1** The different beam-energy  $E_{\text{beam}}$  and target-thickness  $d$  combinations used in the experiment along with the calculated compound nucleus excitation energy  $E_{\text{CN}}$ . The last two columns show the simulated MARA transmission efficiency  $\epsilon_t$  and calculated experimental production cross sections for the  $9^+$  isomeric state  $\sigma_{9^+}$

$E_{\text{beam}}$ [MeV]	$d$ [mg/cm <sup>2</sup> ]	$E_{\text{CN}}$ [MeV]	$\epsilon_t$ [%]	$\sigma_{9^+}$ [mb]
75	0.76	39	4.9(8)	1.5(6)
75	0.45	41	6.3(10)	2.4(9)
80	0.91	42	4.1(7)	1.9(9)
80	0.45	43	6.7(11)	8(3)
87	0.45	48	7.5(12)	7(3)

works, measuring 1.15(4) and 7.9(3)  $\mu\text{s}$  for the half-lives of the  $5^+$  and  $9^+$  states, respectively. They also observed all the same transitions above the  $9^+$  state as in Ref. [20], except the 1998-keV one.

The excited states of  $^{66}\text{As}$  have been studied extensively with various theoretical models using the complex excited Vampir model [22, 23], the interacting boson model [24–26], the deformed shell model [27] and the shell model with an extended P+QQ interaction with monopole corrections [28], the JUN45 interaction [29], and the jj44b interaction [7, 30]. In the shell-model picture, the ground state of  $^{66}\text{As}$  is composed of a coupling of a single neutron and a proton in their respective  $1f_{5/2}$  single-particle orbitals. The  $9^+$  isomeric state has been interpreted to result from a fully aligned  $T = 0$  proton-neutron pair in the  $1g_{9/2}$  orbital, and that the isomerism arises from the breaking of this pair to form the  $7^+$  state to which the  $9^+$  state decays [28–30].

In this article, we report newly observed  $\gamma$ -ray transitions above the  $9^+$  isomer in  $^{66}\text{As}$ , and we extend the two bands known from earlier measurements and add several other new states to the level scheme. Most of the previously observed but unassigned transitions are placed in the level scheme in the current work. The results are compared with shell-model calculations using the JUN45 [29] and jj44b [31, 32] interactions. We also report the absolute recoil- $\beta$  tagging (RBT) efficiency of the Tuike detector [33] for the first time, as the current data is uniquely suited for this determination.

## 2 Experimental methods

The experiment was performed by impinging a  $^{28}\text{Si}$  beam on a self-supporting  $^{\text{nat}}\text{Ca}$  target using the K130 cyclotron at the Accelerator Laboratory of the University of Jyväskylä, Finland. Beam energies of 75, 80, and 87 MeV and targets with thicknesses of 0.45, 0.76, and 0.91 mg/cm<sup>2</sup> were used. The different beam-target combinations are listed in Table 1.

The vacuum-mode separator MARA [34] was used to separate the recoiling fusion-evaporation reaction products (recoils) from the primary beam particles and to distinguish the recoils by their mass-per-charge ( $m/q$ ) values. Physical slits were used in the experiment to suppress the yield of neighbouring masses from arriving at the focal-plane detectors. After MARA, the recoils first passed through a Multi-Wire Proportional Counter (MWPC) and were then implanted into a Double-Sided Silicon strip Detector (DSSD). The DSSD was a Micron BB20 type with a thickness of 300  $\mu\text{m}$ . During the analysis process, the recoils were identified by the energy deposited into the DSSD and their time of flight between the MWPC and the DSSD. The DSSD events without coincidence with the MWPC detector events were defined as decays. The additional ancillary detectors at the focal plane were Tuike [33], a position-sensitive plastic scintillator detector used for detection of  $\beta$  particles, and three broad-energy germanium detectors for  $\gamma$ -ray detection. More detailed descriptions of the focal-plane detectors can be found in Refs. [33,35].

The germanium-detector array JUROGAM 3 [36] at the target area was used to detect promptly emitted  $\gamma$  rays. The full JUROGAM 3 comprises 15 tapered and 24 Clover detectors, and each detector has an individual BGO shield for Compton suppression. In this experiment, one Clover detector was not usable. The detectors in JUROGAM 3 are arranged in four rings at the angles of 75.5°, 104.5°, 133.6°, and 157.6° with respect to the beam direction. Generally, the first two rings are composed of twelve Clover detectors each, while ten and five tapered detectors are in the rings at the angles of 133.6° and 157.6°, respectively. The charged-particle veto detector JYUTube (Jyväskylä-York University Tube), consisting of 120 plastic-scintillator elements, was installed inside the target chamber surrounding the target. JYUTube can be used to aid in selecting the evaporation channel, though it was not utilised in the current analysis.

All detector signals were fed into 100-MHz digitisers and recorded in a triggerless mode. During the analysis, logical events and histograms were formed using a C++ sort code and the spectra were analysed using dedicated Python scripts.

### 3 Results

#### 3.1 Isomer-decay tagging assisted $\gamma$ -ray spectroscopy of $^{66}\text{As}$

Correlating with the electrons emitted within 100  $\mu\text{s}$  after recoil implantation observed at the focal plane proved to be a powerful tool to identify the prompt  $^{66}\text{As}$   $\gamma$ -ray lines from the intensive background caused by more abundantly produced nuclei. The observed conversion electrons show up as a concentration of events with short decay times in

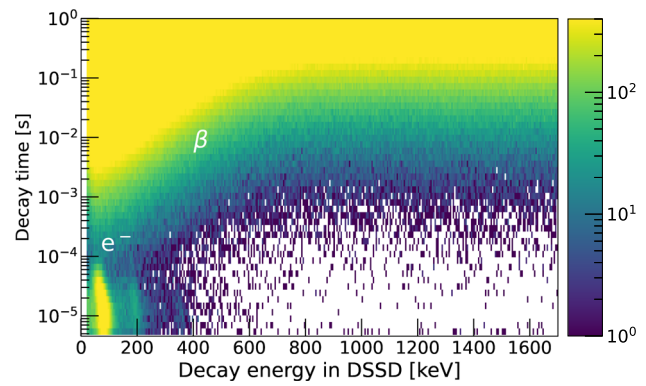


**Fig. 1** Decay time as a function of the decay energy measured in the DSSD. Conversion electron events with short times and low energies are at the bottom left. Most of the spectrum is composed of events from  $\beta$  particles

Fig. 1. However, only the decay of the 7.9- $\mu\text{s}$   $9^+$  isomer could produce a signal that could be separated from the recoil signal. The decay of the 1.15- $\mu\text{s}$   $5^+$  isomer and recoil signals could not, on average, be separated from each other due to the dead time of about 6  $\mu\text{s}$  for processing of the signal of a given DSSD strip. Occasionally, when both isomeric decays occurred through internal conversion, the signals piled up and resulted in a faint but recognisable accumulation of events at an energy around 200 keV as shown in Fig. 1. The calculated K-conversion electron energies for the 124- and 114-keV  $E2$  transitions from the  $5^+$  and  $9^+$  states are 112.5 and 102.5 keV, respectively. The corresponding K-conversion coefficients are  $\alpha_K = 0.42$  and 0.31 [21]. A recoil-gated prompt JUROGAM 3  $\gamma$ -ray spectrum is shown in Fig. 2a, where the most significant peak at 191 keV originates from the  $5/2_1^- \rightarrow 3/2_{g.s.}^-$  transition in  $^{65}\text{Ga}$ . By setting an upper limit of 0.1 ms on the observed recoil-decay time differences, in panel (b) of the same figure, all the visible  $\gamma$ -ray peaks from strong fusion channels shown in panel (a) have disappeared from the prompt  $\gamma$ -ray spectrum, including the aforementioned 191-keV transition. For both spectra, the randomly correlated background was removed by using a temporal recoil-JUROGAM 3 correlation window, which was placed outside the real recoil- $\gamma$  correlation time distribution. In fact, it will be later shown in Sect. 3.3 that all peaks left in Fig. 2b originate from the de-excitation of the excited states above the 7.9- $\mu\text{s}$ ,  $9^+$  isomer in  $^{66}\text{As}$ . In the following, a “conversion-electron tag” refers to the applied 0.1-ms recoil-decay correlation time gate.

The proposed level scheme of  $^{66}\text{As}$  above the  $9^+$  state is shown in Fig. 3. The assignments of the newly observed states and transitions are based on  $\gamma$ - $\gamma$  coincidences, energy sums of the observed transitions, and relative  $\gamma$ -ray intensities. Details of all the  $\gamma$ -ray transitions observed in Fig. 2b are listed in Table 2, where the quoted intensities are relative to the intensity of the 841-keV transition that feeds the isomeric

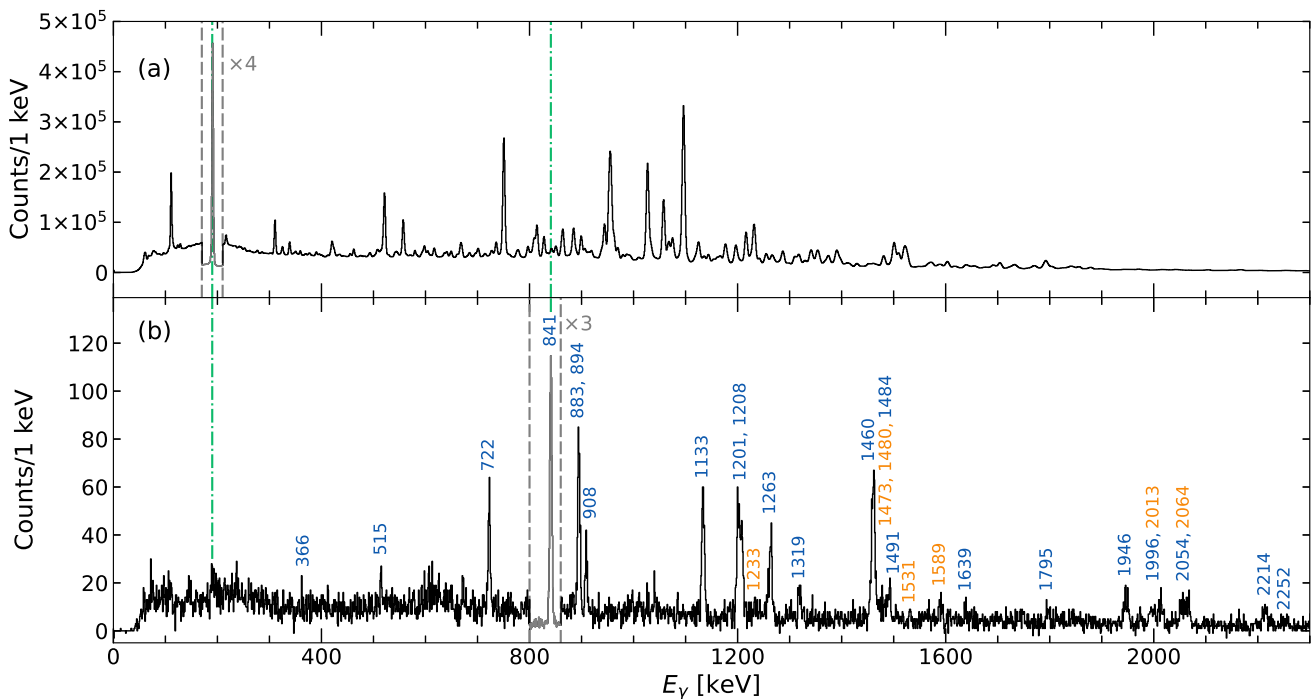


**Fig. 2** Prompt JUROGAM 3  $\gamma$ -ray spectrum requiring detection of **a** a recoil and **b** a recoil and a conversion electron. The random background in the recoil- $\gamma$  time gate has been removed from both spectra. To enhance the legibility of the spectra, the y axes have been scaled down in the regions marked with grey dashed lines by the factors of four and

three in panels **a** and **b**, respectively. Transitions labelled in blue have been placed in the level scheme of  $^{66}\text{As}$ , while the orange labels indicate transitions originating from  $^{66}\text{As}$ , but which are not placed in the level scheme. The peak-like structures without labels in panel (**b**) are considered to be random single-bin statistical fluctuations

state. The spins and parities for the isomer and the two states placed directly above it have been adopted from the works presented in Refs. [20,21]. Other spin values included in Fig. 3 have been determined using angular distribution ratios, which are discussed in detail later in this section. While the current experimental data does not allow to deduce the parities of the excited states, based on the discussion presented in Sect. 4, parities have been suggested for specific states. The excitation energy of the isomeric  $9^+$  state was determined to be 3022.77(10) keV based on the measured energies of the delayed  $\gamma$  rays observed at the MARA focal plane.

The structure built above the  $9^+$  isomer in  $^{66}\text{As}$  is investigated using  $\gamma$ - $\gamma$  coincidence analysis. Conversion-electron tagged coincidence spectra with coincidence gates on the 722- and 1460-keV lines are shown in Fig. 4a and b, respectively. These lines are not in mutual coincidence, but their respective coincident spectra show many of the same lines, indicating two cascades of transitions with energies of 722–841–894–1263–1946 and 841–894–1208–1263–1460 keV. The 894-keV transition is a new addition, and the details will be discussed in the next paragraph. Furthermore, concurrently gating on the 722-, 894-, and 1263-keV lines, see Fig. 4c, reveals an additional line at 1996 keV, originally observed by Grzywacz et al. [20]. A statistically significant line with an energy of 1639 keV is also observed in the same

spectrum, and due to its small intensity the corresponding transition is placed to feed the state de-excited by the 1996-keV transition.

Figure 5 shows a  $\gamma$ -ray spectrum with the conversion-electron tag and a coincidence gate on the 894-keV transition. All the abovementioned transitions with energies of 722, 841, 1208, 1263, 1460, and tentatively 1996 keV are seen in the spectrum. It is important to note that the line at 894 keV is in coincidence with both the 722–1946 and 1208–1460 keV pairs, indicating that it must be located either above or below the parallel-running structures in the level scheme. Because the 894-keV transition has a higher intensity than the 1263-keV one, it is placed to feed the state at 6531 keV. This changes the structure previously proposed by Grzywacz et al. [20] and Ruotsalainen et al. [21], where the state at 6531 keV was assigned to be fed directly by the 1263-keV transition. Interestingly, the 894-keV line was observed in both studies but could not be placed in the level scheme. Contrary to the previous observations made in Ref. [20], the present data clearly shows a coincidence between the 1208- and 894-keV transitions, which further supports the current placement of the latter one.

Figure 6a shows conversion-electron tagged  $\gamma$  rays coincident with the new line at 1795.4(13) keV demonstrating coincidences with the 841- and 1460-keV transitions. There-

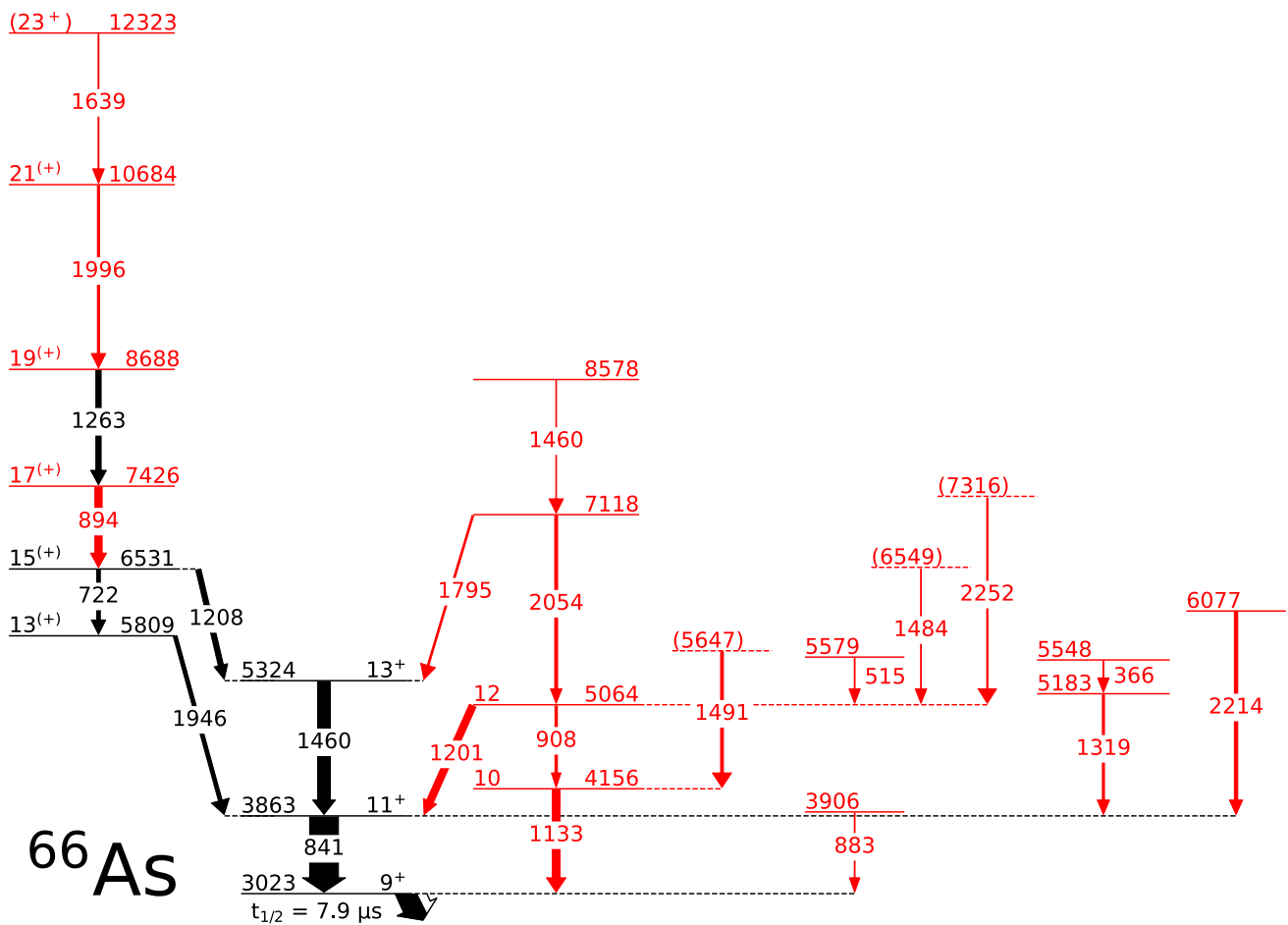


**Fig. 3** Proposed level structure above the  $9^+$  isomeric state in  $^{66}\text{As}$ . The newly observed transitions and levels are coloured in red. Tentative transitions and levels are dashed. The widths of the arrows indicate intensities relative to the 841-keV transition. The lifetime of the  $9^+$ , 3023-keV isomeric state was taken from Ref. [21], and its energy is

determined using the energies of the delayed  $\gamma$  rays observed by the focal plane germanium detectors. The spins and parities of the isomer and the two states directly above it have been taken from earlier works [20,21]

fore, the 1795-keV transition is placed to populate the known  $13^+$  state at 5324 keV. Figure 6b and c show the transitions in coincidence with the 1201- and 2054-keV lines, respectively. It should be noted that the 1201-keV line forms a doublet with the 1208-keV line, the latter of which has already been placed in the level scheme, though the line was reported to be unusually wide in Ref. [20]. From the coincidence spectra, one observes that both 1201- and 2054-keV lines are coincident with the 841-keV transition as well as with each other. The transitions at 1201 and 2054 keV are, therefore, deduced to form a cascade feeding the known  $11^+$  state at 3863 keV and their order is decided based on their intensities. The energy sum of the 1460-1795-keV and 1201-2054-keV cascades is the same, which suggests that the cascades run parallel starting from the same state at 7118 keV. Both 1201- and 2054-keV transitions show a coincidence with a line at 1460-keV, which is placed to feed the state at 7118 keV. The

panel b in Fig. 6, i.e., the  $\gamma$ -ray spectrum in coincidence with the 1201-keV transition, shows additional lines at 515 and 1484 and one count at 2252 keV. Figure 6d shows further support for the 2252-keV transition being coincident with the 1201-keV transition. No mutual coincidence is observed between the 515-, 1484-, and 2252-keV transitions nor with the 2054- or 1460-keV transitions, so these three transitions are tentatively placed to parallelly precede the 1201-keV transition and feed a newly discovered state at 5064 keV.

A transition with an energy of 1133 keV, while relatively intense in the conversion-electron tagged singles spectrum of Fig. 2, does not show particularly strong coincidences with other transitions. However, a tentative coincidence with a less-intense 908-keV line is observed. Because the two sum up to the new 5064-keV state, they are added to the level scheme to run parallel with the 1201- and 841-keV transitions, with the 1133-keV transition directly populating

**Table 2** List of the all  $\gamma$ -ray transitions associated with  $^{66}\text{As}$  above the  $9^+$  isomer in Fig. 2b using the conversion-electron tag.  $E_\gamma$  denotes the transition energy,  $I_{\text{rel}}$  the relative intensity of the transition, and  $E_i$  and  $E_f$  are the energies of the initial and final state, respectively.  $R$  is the intensity ratio of  $\gamma$ -rays as explained in the text

$E_\gamma$ [keV]	$I_{\text{rel}}$ [%]	$E_i$ [keV]	$E_f$ [keV]	$R$
365.7(10)	< 2 <sup>1</sup>	5548.2(15)	5182.5(12)	
514.5(8)	2.6(4)	5578.8(11)	5064.2(7)	
721.9(7)	12.6(9)	6531.3(9)	5809.4(12)	1.07(12)
840.5(7)	100(4)	3863.3(7)	3022.77(10)	1.14(6)
882.7(12)	2.4(4)	3905.5(12)	3022.77(10)	
894.3(7)	25.2(14)	7425.6(11)	6531.3(9)	1.44(15)
908.4(8)	8.3(8)	5064.2(7)	4155.9(7)	1.2(2)
1133.1(7)	27(2)	4155.9(7)	3022.77(10)	0.97(12)
1200.8(8)	24.6(15)	5064.2(7)	3863.3(7)	0.76(9)
1207.7(8)	17.9(13)	6531.3(9)	5323.5(10)	1.34(15)
1233.3(11)	4.2(6)			
1262.6(7)	18.2(13)	8688.2(13)	7425.6(11)	1.12(15)
1319.2(9)	7.1(8)	5182.5(12)	3863.3(7)	
1460.3(14)	< 2 <sup>1</sup>	8578(3)	7118.4(11)	
1460.3(7)	44(3)	5323.5(10)	3863.3(7)	1.30(13)
1473(3)	4.3(7)			
1480(3)	4.0(7)			
1484(3)	< 2 <sup>1</sup>	6549(3)	5064.2(7)	
1491.0(10)	9.5(10)	5646.9(12)	4155.9(7)	
1531(3)	2.1(5)			
1589.3(15)	4.1(7)			
1639(3)	2.7(6)	12323(3)	10684(2)	
1795.4(13)	5.6(8)	7118.4(11)	5323.5(10)	
1946.2(10)	12.8(13)	5809.4(12)	3863.3(7)	1.6(3)
1996.2(13)	7.5(10)	10684(2)	8688.2(13)	1.4(5)
2012.9(11)	11.4(13)			1.1(4)
2053.6(14)	9.9(12)	7118.4(11)	5064.2(7)	1.0(4)
2064.4(13)	11.6(13)			0.5(3)
2213.5(11)	11.5(13)	6076.8(12)	3863.3(7)	
2252(2)	4.1(8)	7316(2)	5064.2(7)	

<sup>1</sup>Transition was observed only in coincidences and therefore only an upper limit is given

the  $9^+$  isomeric state. Additionally, a line with an energy of 1491 keV is observed to be tentatively in coincidence with the 1133-keV transition but not with the 908-keV one. Therefore, the 1491-keV transition is assigned to run parallel with the 908-keV transition. The 908- and 1133-keV lines were also observed in Refs. [20,21] but were not placed in the level scheme.

The transition at 883 keV is observed to have no clear coincident transitions so it is placed to feed directly the isomeric state, parallel to 1133- and 841-keV transitions. Transitions of 1319 and 366 keV are observed in coincidence with the 841-keV transition, and therefore they are set to form a cascade feeding the 3863-keV  $11^+$  state. Another transition at

2214 keV is confirmed to be in coincidence only with the 841-keV transition due to low statistics.

Finally,  $\gamma$ -ray transitions with the energies of 1531, 1589, 2013, 2064, 1233, 1473, and 1480 keV, observed in the conversion-electron tagged singles spectrum of Fig. 2, are not placed in the level scheme due to low statistics. The first five appear to be in coincidence with the 841-keV transition. The last two lines are located in an energy range where there are several transitions with similar energies, and as such, no clean gates could be made, nor did they appear in coincidence with the other transitions. The 2013-keV transition was also observed in the earlier work by Grzywacz et al. [20].

In order to obtain some confidence for the spin assignments for the excited states above the  $9^+$  isomer in  $^{66}\text{As}$ , the

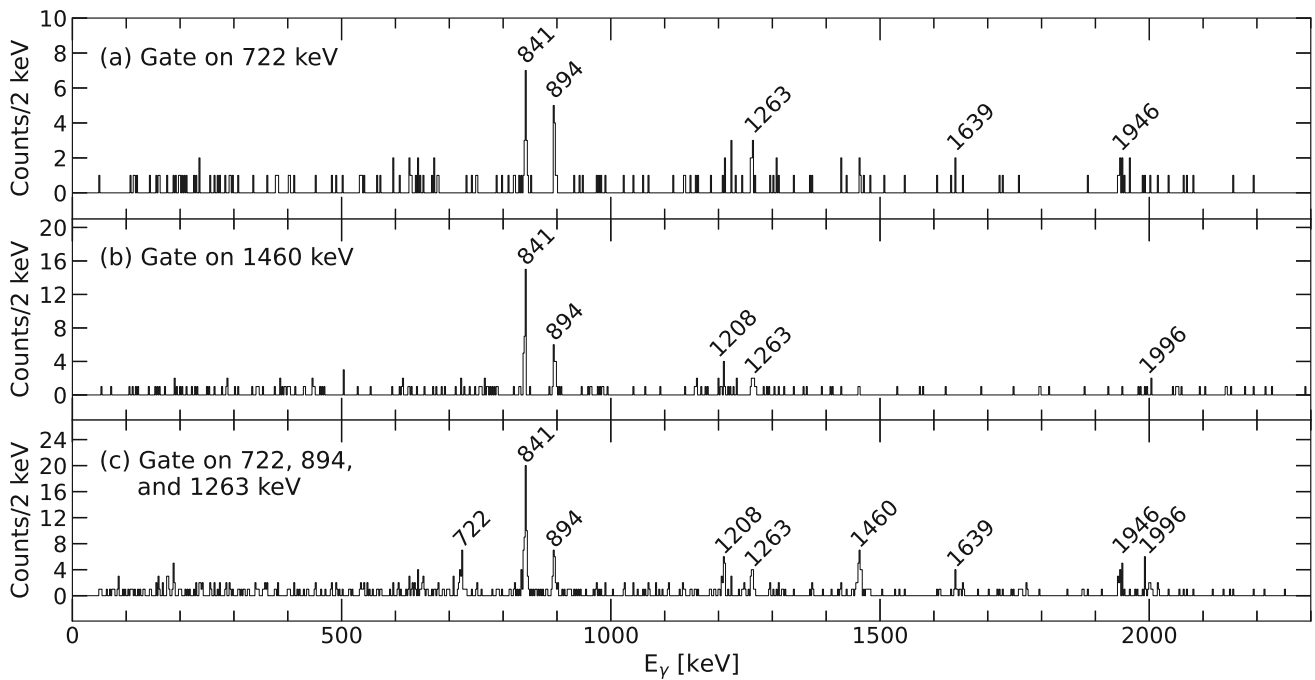


**Fig. 4** Conversion-electron tagged prompt  $\gamma$ - $\gamma$  projection spectra in coincidence with the **a** 722-keV, **b** 1460-keV, and **c** concurrently on the 722-, 894-, and 1263-keV transitions

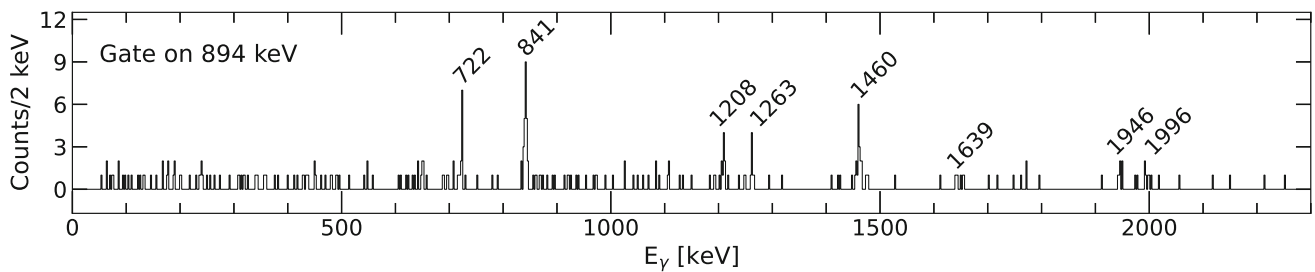


**Fig. 5** Conversion-electron tagged prompt  $\gamma$ -ray spectrum in coincidence with the 894-keV  $\gamma$ -ray transition

angular distribution ratios (the  $R$  values) have been investigated in the present work. The  $R$  values, defined here as  $R = 2I_\gamma(157.6^\circ + 133.6^\circ)/[I_\gamma(104.5^\circ) + I_\gamma(75.5^\circ)]$ , can be used to deduce the  $\gamma$ -ray transition multipole orders. This was done so that the intensity of the investigated  $\gamma$ -ray line was determined in the recoil-electron-tagged spectra divided into three different JUROGAM 3 rings as shown by the equation and then corrected for detection efficiencies before the angular distribution ratio  $R$  was calculated. The data from rings at angles  $157.6^\circ$  and  $133.6^\circ$  were combined and treated as a single ring. Reference values for a stretched quadrupole ( $\Delta J = 2$ ) and a stretched dipole ( $\Delta J = 1$ ) transitions were determined to be 1.22(1) and 0.82(2), respectively, from known  $E2$  and  $M1$  transitions in  $^{65}\text{Ga}$ . The angular distribution ratios and transition multipole orders have been determined for those transitions in  $^{66}\text{As}$  with sufficient statistics and the former are listed in Table 2.

The transitions with energies of 841 and 1460 keV have angular distribution ratios of  $R = 1.14(6)$  and  $1.30(13)$ , respectively, which suggests they both have a quadrupole character. This is in agreement with the earlier observations made in Refs. [20,21]. In contrast, the 1208-keV transition is determined to have a stretched quadrupole character in the present work. This observation is significant as it will alter the spins of the yrast band, which were previously assigned in Refs. [20,21] to have even values. The significance of this change will be discussed further in Sec. 4. Additionally, we have an indication that the 1133-keV transition has a dipole character, and so the state at 4156 keV has been assigned as  $J = 10$ . The 908-keV transition connecting the 5064- and 4156-keV states has a quadrupole character, and as the 1201-keV transition connecting the 5064-keV state to the known  $11^+$  state has a dipole character, the state at 5064 keV has been assigned a spin of 12.



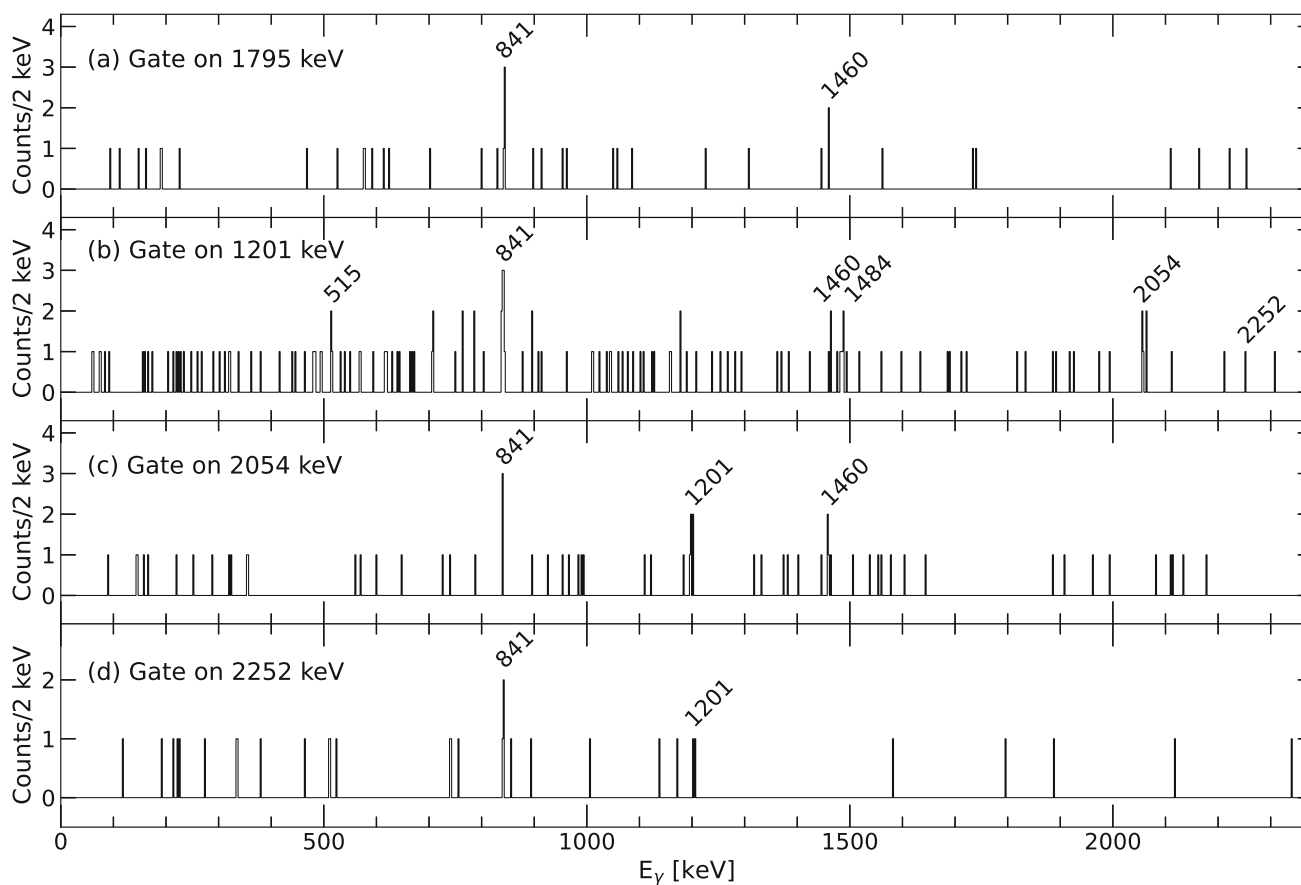


**Fig. 6** Conversion-electron tagged prompt  $\gamma$ -ray spectra in coincidence with transitions with energies of **a** 1795, **b** 1201, **c** 2054, and **d** 2252 keV

### 3.2 Transmission of MARA and the production cross section of the $9^+$ state in $^{66}\text{As}$

Transmission values of MARA for the  $^{66}\text{As}$  The word runs outside the column. Latex struggles with this word often. Hyphenation is evap-o-ra-tion residues were estimated with a Monte-Carlo approach, which consisted of the following steps: (1) energy loss and scattering simulation of primary beam particles to random depths into the target with TRIM [37,38], (2) fusion-evaporation reactions with an isotropic emission of protons and neutrons in the center-of-mass system, (3) energy loss and scattering simulations of the recoils exiting the target with TRIM, (4) sampling of the atomic charge states for the recoils, and 5) third-order transfer-matrix based ion-optical simulation of the products travelling through the MARA separator to the focal-plane setup, including the realistic physical dimensions of the MARA vacuum chambers and the DSSD. In steps 2, 4, and 5 a purpose-made Python code was used. The production cross section of  $^{66}\text{As}$  was assumed to be constant over the target. However, this assumption does not hold very well for the thickest target used in the experiment. Hence, the valid-

ity of this transmission value contains some imprecision. The obtained transmission values are listed in Table 1.

The production cross sections for the  $9^+$  state in  $^{66}\text{As}$  for each beam-target combination were determined using the numbers of conversion electrons observed in the DSSD, corrected for their detection efficiency, the numbers of beam particles that hit the target and consequently caused a reaction, the MARA transmission values, conversion coefficient, and target thicknesses. The numbers of particles hitting the target were estimated from the measured recoil rates, which were normalised with respect to the occasionally measured beam intensities. For the conversion-electron detection efficiencies, the geometrical efficiency, the effect of the dead time of the DSSD, and the flight times through MARA were taken into account. The geometrical DSSD detection efficiency was assumed to be 50%, since the recoils are expected to have shallow implantation depths due to their fairly low kinetic energies and, hence, the electrons emitted into backward angles will escape the DSSD. Due to the limitation imposed by the data acquisition dead time for a DSSD strip, the number of observed electrons needs to be corrected according to the measured recoil-electron time distribution, which yielded the shortest detectable time differ-

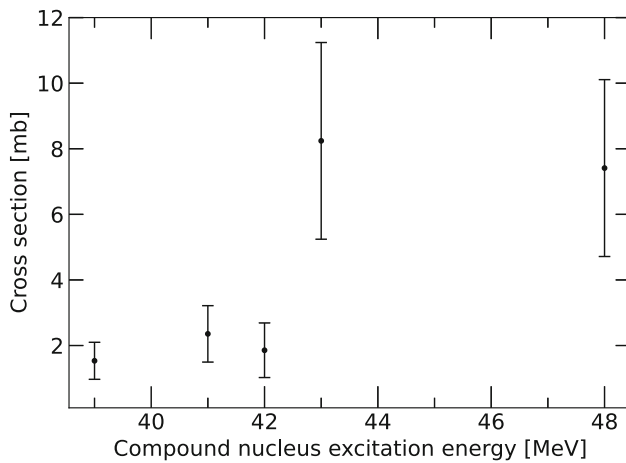


**Fig. 7** Measured production cross section of the  $9^+$  isomeric state in  $^{66}\text{As}$  as a function of the compound nucleus excitation energy

ence between the recoil implant and the conversion electron. For this correction, the half-life of  $7.9(3) \mu\text{s}$  of the  $9^+$  state obtained in Ref. [21] and the exponential decay law were used. This correction was further investigated and confirmed with a Monte-Carlo simulation, which used the literature lifetime and an estimate of the DSSD time resolution of  $1 \mu\text{s}$  for low-energy events. The observed recoil-electron and recoil- $\gamma$  time distributions measured at the focal plane support the earlier measurements of the  $9^+$  isomeric state half-life. The fraction of conversion electrons not observed due to the  $9^+$  isomeric state de-exciting during in-flight within the MARA separator was evaluated using the calculated flight times and the exponential decay law. Finally, the total conversion coefficient of  $0.41(13)$  from [21] was used to take into account that only a part of the decays happened via internal conversion. The cross-section results are listed in Table 1, and the corresponding cross-section plot is shown in Fig. 7. An abrupt increase in the population of the  $9^+$  isomeric state is evident at around an excitation energy between 42 and 43 MeV.

### 3.3 $\beta$ -tagging efficiency of Tuike and purity of the conversion-electron tag

The ground state of  $^{66}\text{As}$  has a half-life of  $T_{1/2} = 96 \text{ ms}$  [39], and it decays via  $\beta$  decay with an end-point energy of  $Q_\beta = 9582 \text{ keV}$  [40]. These properties enable the recoil- $\beta$  tagging (RBT) method to be employed to study this nucleus, and this has indeed been done before in the most recent experimental study of  $^{66}\text{As}$  [21]. However, the efficiency of  $\beta$  tagging has been difficult to determine as  $\gamma$ -ray transitions from the exotic nucleus cannot typically be observed from the background without applying the recoil- $\beta$  tagging conditions. For example, in Refs. [15, 33], the only way to find a hint of the nucleus of interest in the prompt  $\gamma$ -ray spectra

was to require a decay within a suitable correlation time in the DSSD.

In the present study, it is finally possible to determine the  $\beta$ -tagging efficiency because of the unique situation with  $^{66}\text{As}$ : this nucleus can be identified from the data using only conversion-electron correlations or recoil-electron- $\beta$  correlations. By using the numbers of recoil-electron and recoil-electron- $\beta$  chains in the DSSD, requiring also an event in the Tuike detector [33] for the  $\beta$  particle, a ratio of the latter to the former gives a value of  $R = 0.155(2)$ , which translates to a  $\beta$ -tagging efficiency of  $\epsilon_{\text{tag,max}} = 15.5 \%$  with no further conditions on the detected  $\beta$ -particle energy. Therefore, this value should be taken as the highest possible tagging efficiency when incorporating Tuike. However, recoil- $\beta$  tagging analyses typically require the use of stricter  $\beta$ -particle energy conditions (with a lower limit of 2–5 MeV and an upper limit of 10 MeV) to reach sufficient cleanliness in the tagged  $\gamma$ -ray spectra. Consequently, the practical tagging efficiency is further reduced from the quoted value of  $\epsilon_{\text{tag,max}}$ , depending on the shape of the  $\beta$ -particle energy distribution and which portion of the distribution is covered by the set gate.

In addition, the cleanliness of the conversion-electron tagging, meaning that the observed conversion electrons are originating from  $^{66}\text{As}$  only, was verified with the following method. At first, a ratio for the number of correlated conversion electrons in the recoil-electron- $\beta$  and recoil-electron correlations was found to be  $0.227(3)$ . Here, the correlation required a conversion electron within 0.1 ms after the recoil, and a  $\beta$  decay in the DSSD within 300 ms after the conversion electron, but the  $\beta$  particle did not need to be observed in Tuike. Then, the intensity ratio for the prompt 841-keV  $\gamma$ -ray transitions feeding the  $9^+$  isomer was extracted from two  $\gamma$ -ray energy spectra employing the same recoil-electron- $\beta$  and recoil-electron correlations. The obtained ratio is  $0.215(13)$ , which agrees within uncertainty with the ratio calculated from the number of correlated conversion electrons. This result implies that essentially all observed conversion electrons must originate from the decay of the  $9^+$  isomer in  $^{66}\text{As}$ . Therefore, the observed conversion-electron tagged  $\gamma$ -ray transitions can be unambiguously associated with  $^{66}\text{As}$ .

## 4 Discussion

In Ref. [20] the yrast sequence containing the 722-, 1262-, and 1998-keV transitions was assigned to have an even spin. The reason for this was the assumed stretched dipole ( $E1$  or  $M1$ ) character for the 1208-keV transition. It was noted in Ref. [20] that the line at 1208 keV “is broader than the neighboring lines at 1131 and 1262 keV” and “such an angular dependence effect can be produced e.g. if there is a closely spaced doublet of  $E2$  and  $E1/M1$  lines near 1208 keV”. Even if the potential doublet nature of the 1208-keV transition was

recognized in Ref. [20], only the 1208-keV transition with assumed dipole character was placed in the level scheme fixing the spins of the higher lying levels to even spin. The work presented in Ref. [21] focused on the spectroscopy of the low-lying states in  $^{66}\text{As}$ , but employing the isomer-tagging method, the strongest transitions above the  $9^+$  isomer were also observed in that work. Based on the extracted angular distribution ratios (the  $R$  values) in Ref. [21], quadrupole character was deduced for the 841-, 1460-, and 722-keV transitions and dipole character for the 1208-keV transition. It should be noted that the 1208-keV transition in Ref. [21] was not considered to be a doublet.

The doublet nature of the 1208-keV and 1201-keV transitions has been confirmed in the present work and both transitions have been placed in the level scheme. In contrast to the earlier publications of Refs. [20,21], the 1208-keV transition is determined to have a stretched quadrupole character in the present work. Conversely, the newly placed 1201-keV transition appears to be a dipole. It is likely that the even-spin assignment of the highest-energy levels in the earlier works is due to the doublet nature of the 1201/1208-keV transitions. As observed in the present work, the 1208-keV transition appears more strongly in coincidence with the other transitions, while the 1201-keV transition dominates the singles  $\gamma$ -ray spectrum. Therefore, the multipolarity estimations in the previous works might have been dominated by the 1201-keV line leading to a wrong conclusion. Moreover, considering that the 1946-keV transition also shows a quadrupole character, these observations reveal that the left-most band in Fig. 3 is an odd-spin sequence instead of the even spin as previously assigned in Refs. [20,21]. Therefore, we have assigned  $J = 13$  for the state at 5809 keV,  $J = 15$  for the state at 6531 keV, and so on.

In the level scheme, the states above the  $9^+$  isomer in  $^{66}\text{As}$  can be divided into two groups: the bands with a rotation-like structure (left in Fig. 3) and the scattered states typical for an odd-odd nucleus. While the bands are relatively easy to compare with the theoretical models, the scattered states are more difficult to connect to any specific calculated states. This is further complicated by the fact that the multipolarities could not be extracted for the transitions connecting the scattered states due to low statistics.

As the excitation energy is increased, the gain in angular momentum splits at  $J = 13$  (on the left in the level scheme of Fig. 3). The simple assumption is that the yrast  $11^+$  and  $13^+$  states have the same structure, namely that of the isomeric  $9^+$  state. Additionally, it can be supposed that the  $J = 15$  and  $J = 13$  states, connected by the 722-keV  $E2$  transition, have the same or similar structures since the competing 1208-keV higher-energy transition from the  $J = 15$  state to the yrast  $J^\pi = 13^+$  state does not capture all of the decay intensity. Correspondingly, there may be additional  $J = 11$  and  $J = 9$  states below the  $J = 13$ , 5809-keV state belonging to the

same cascade, but as the associated  $\gamma$ -ray transitions have probably lower energies than the observed 1946-keV transition, this higher-energy transition to the yrast  $J^\pi = 11^+$  state dominates and leaves the non-yrast  $J = 11$  and  $J = 9$  states unobserved. Other  $9^+$  states have been observed in Ref. [21], and potential feeding to these states, for example from the 5809-keV  $J = 13$  state, must bypass the isomeric the  $9^+$  state. However, in the current work, no such transitions to the non-isomeric  $9^+$  states were observed when using the recoil- $\beta$  or recoil-isomeric- $\gamma$  tagging methods.

It should be noted that there is no definite experimental information on the parities of the states above the  $9^+$  isomer. The positive parity for the isomer itself stems from the assumed  $\pi(1g_{9/2})^1 \otimes \nu(1g_{9/2})^1$  configuration [19,29]. On this basis, the states at 3863 keV and 5324 keV, likely belonging to the same multiplet as the  $9^+$  isomer, have also been assigned positive parities. Moreover, the neighboring odd-odd  $N = Z$  nuclei, such as  $^{58}\text{Cu}$  [41],  $^{62}\text{Ga}$  [4] and  $^{70}\text{Br}$  [42], all show that the yrast bands at high excitation energy are odd spin and positive parity. A negative parity assignment for the sequence starting from the 5809-keV state would imply an  $M2$  character for the 1208- and 1946-keV transitions. However, this is not very likely as the 722-keV transition with an assumed  $E2$  character would then dominate over such a  $M2$ , 1208-keV transition, whereas the two transitions are observed to have similar intensities. Further insight to the structure of  $^{66}\text{As}$  can be obtained from comparisons to the shell-model calculations using both *jj44b* and *JUN45* interactions.

Large-scale shell-model calculations have been performed using both the *JUN45* [29] and the *jj44b* [31,32] effective interactions with a  $^{56}\text{Ni}$  core. The model space consists of  $1f_{5/2}2p1g_{9/2}$  proton and neutron orbitals between shell closures at 28 and 50. The *JUN45* interaction is constructed by initially utilizing a realistic interaction derived from the Bonn-C potential, followed by empirical adjustments to the single-particle energies of the four orbitals and 133 two-body matrix elements [29]. The *JUN45* interaction has previously been employed to investigate the structures of  $N = Z$  nuclei (see, e.g., Ref. [2]), but it has also been used for the nuclear moments [43],  $\beta$ -decay [44,45], and double  $\beta$ -decay [46] studies.

The *jj44b* Hamiltonian was derived by fitting approximately 600 binding energies and excitation energies using a method similar to that employed for the *JUN45* Hamiltonian [29]. With varying 30 linear combinations of the good  $J - T$  two-body matrix elements, the root-mean-square deviation between experimental and theoretical energies in the fit was approximately 250 keV [31,32]. The single-particle energies of the included proton and neutron orbitals are taken as  $E_{sp}(f_{5/2}) = -9.2859$  MeV,  $E_{sp}(p_{3/2}) = -9.6566$  MeV,  $E_{sp}(p_{1/2}) = -8.2695$  MeV, and  $E_{sp}(g_{9/2}) = -5.8944$  MeV. The present calculations have been performed in the

full model space without any truncation. In this study, the shell-model code KSHELL [47] was employed to diagonalize the shell-model Hamiltonian matrices. The  $B(E2)$  values were calculated using the effective charges  $e_p = 1.5e$  and  $e_n = 0.5e$ , and the  $B(M2)$  values using the gyromagnetic ratios  $g_s^p = 5.585$  and  $g_s^n = -3.826$ .

A comparison between the two leftmost bands in the level scheme of Fig. 3 and the results of the shell-model calculations using both the jj44b and JUN45 interactions is presented in Fig. 8. The calculated states selected for comparison are based on the largest  $B(E2)$  values connecting the levels. The jj44b interaction underestimates the excitation energy of the  $9^+$  isomer by 1.065 MeV, while the corresponding state in the JUN45 calculation is 0.517 MeV below the experimental value. The experimental level spacings between the yrast  $11^+ - 9^+$  and  $13^+ - 11^+$  states are reasonably well reproduced by both interactions. The experimentally observed sequence starting from the 5809-keV state is compared to the calculated odd-spin positive- and negative-parity states. It is apparent that the calculated states have too high excitation energies with respect to the experimental counterparts. Such overestimations, specifically with the JUN45 interaction, were also noted in Ref. [29], for example, for the prolate deformed band in  $^{68}\text{Se}$ . The insufficiency of the model to correctly describe the prolate shapes was attributed to the missing  $2d_{5/2}$  orbit in the model space. Therefore, the observed  $J = 13 - 23$  band in  $^{66}\text{As}$  may be prolate deformed explaining the rather poor agreement with the presented calculations. Interestingly, in both calculations the odd-spin negative-parity states become yrast at  $J^\pi = 17^-$ .

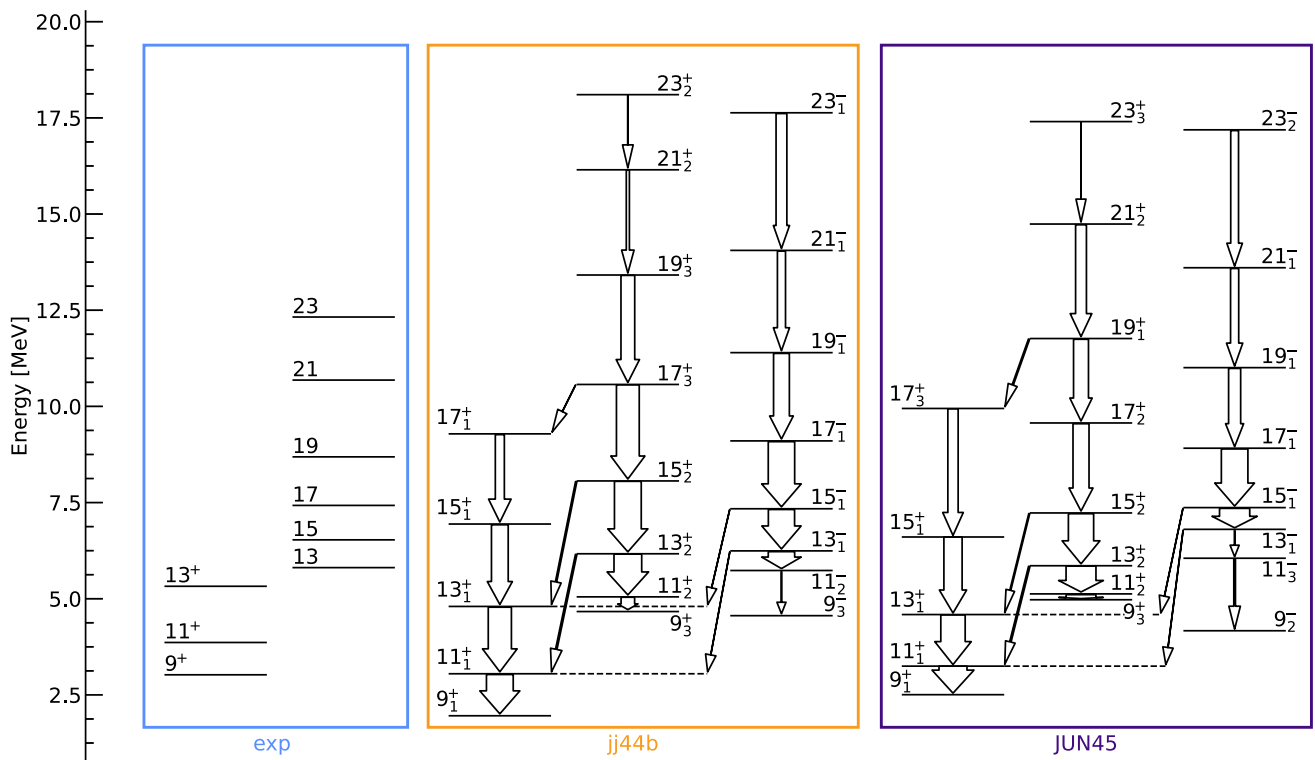
The transitions that connect the  $J = 15$  state to the two  $J = 13$  states, i.e., the observed 722- and 1208-keV transitions, are crucial in determining the parity of the odd-spin yrast sequence starting from the 5809 keV state. In the case of a positive parity, the deduced branching ratios for the 722- and 1208-keV transitions, based on the calculated  $B(E2)$  values, yield values of 61% (66%) and 39% (34%) for the jj44b (JUN45) interaction, respectively. Assuming that the 6531-keV state is a negative-parity  $J = 15$  state, the calculated  $B(E2)$  and  $B(M2)$  values of both interactions indicate that it should be depopulated almost exclusively by the 722-keV in-band transition, at variance with the experimental observations. Therefore, the calculated branching ratios without a parity change are in better agreement with the experimental intensities, considering that the intensity of the 722-keV transition can be only partially observed as the potential subsequent transitions may bypass the  $9^+$  isomer. Based on this discussion, the yrast odd-spin sequence most likely has a positive parity as indicated in Fig. 3.

The shell-model calculations also support the interpretation that the observed non-yrast  $J^\pi = 13^{(+)}$  state has a structure more closely related to that of the  $J^\pi = 15^{(+)}$  state: As is evident from the calculated transition strengths in Fig. 8, the

$B(E2; 15_2^+ \rightarrow 13_2^+)$  value is considerably larger than that for the  $15_2^+ \rightarrow 13_1^+$  transition, implying a larger overlap of the wavefunctions for the first transition than for the second. This is true for both interactions. It was hypothesised purely from the experimental data that even if an additional  $J^\pi = 11^{(+)}$  state with a similar structure to that of the left-most band in Fig. 3 exists, the energy of the transitions de-exciting the second  $J^\pi = 13^{(+)}$  state plays an important role in deciding the de-excitation path. This is also predicted by the calculations: the  $13_2^+ \rightarrow 11_2^+$  transition may have a significantly larger  $B(E2)$  value than that of the  $13_2^+ \rightarrow 11_1^+$  transition, but the calculated energy of the latter is approximately three times higher.

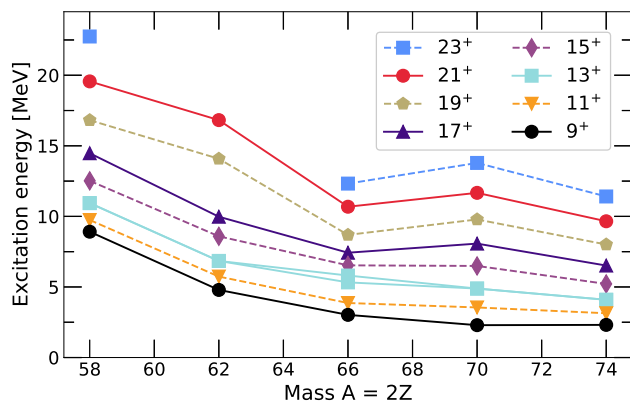
Another interesting experimental observation is the backbend between  $J^\pi = 21^{(+)}$  and  $J^\pi = (23^+)$  in the left-most band of the level scheme. The backbend at these spin values is reproduced in both calculations for the positive-parity states, but it should be noted that there are backbends and upbends also at lower spin values in the calculated level schemes. There is no backbend in either calculated negative-parity band. For the states of both calculated positive-parity bands, the configuration with the highest amplitude is  $(1f_{5/2})^2(2p_{3/2})^2(2p_{1/2})^0(1g_{9/2})^1$  for both protons and neutrons, and its portion of the wave function increases as the spin increases. The maximum spin this configuration can create is  $J_{\text{max}} = 21$ . To generate more angular momentum, in both calculations, an additional neutron and proton have been excited to the  $1g_{9/2}$  orbital. However, it is not obvious whether there are now two (isoscalar) neutron-proton pairs or a neutron-neutron and proton-proton pair. Nevertheless, the experimentally observed backbend may be related to the increased occupancy of the  $1g_{9/2}$  orbital. It is also noteworthy that the calculated  $B(E2)$  values in the positive-parity bands reduce constantly, which is indicative of an approaching termination.

Figure 9 shows the systematics of the  $9^+ - 23^+$  states in the odd-odd  $N = Z$  nuclei between  $^{58}\text{Cu}$  and  $^{74}\text{Rb}$ . For  $^{66}\text{As}$  the experimentally observed states up to  $J^\pi = (23^+)$  have been included despite the parities for the higher-lying states are not experimentally fixed. With increasing mass number, energies of all states decrease as the midshell is approached and exciting a nucleon to the  $1g_{9/2}$  orbital requires less energy. The evolution is smooth especially for the  $9^+$  states, but the higher-lying states show clear differences. In  $^{62}\text{Ga}$  the odd-spin yrast band terminates at  $J^\pi = 17^+$ , which is reflected by the increased level spacing between the  $17^+$  and  $19^+$  states. Such termination effects are not visible in the heavier nuclei. In  $^{66}\text{As}$ , the level sequence from the second  $J^\pi = 13^{(+)}$  state onwards shows perhaps a more abrupt drop in terms of the excitation energies, which may hint towards a structural change for these states in comparison to neighboring isotopes. In  $^{70}\text{Br}$  the excitation energies increase in comparison to  $^{66}\text{As}$  and they reduce when reaching  $^{74}\text{Rb}$ . In  $^{70}\text{Br}$



**Fig. 8** Comparison between the experimentally determined level energies in  $^{66}\text{As}$  and those calculated with the shell model using the *jj44b* and *JUN45* interactions. The widths of the arrows represent the calcu-

lated  $B(E2)$  and  $B(M2)$  values in the units of W.u. The bands have been constructed by selecting the largest  $B(E2)$  values connecting the levels



**Fig. 9** Systematics of the  $9^+ - 23^+$  states in the odd-odd  $N = Z$  nuclei in the *fp* shell. Both  $J = 13^+$  states in  $^{66}\text{As}$  have been included. Data on  $^{58}\text{Cu}$  [41,49],  $^{62}\text{Ga}$  [5],  $^{70}\text{Br}$  [42], and  $^{74}\text{Rb}$  [48] are from the given references

and  $^{74}\text{Rb}$ , these bands have been interpreted to have prolate deformations [42,48], and the same may be true for  $^{66}\text{As}$  as discussed above. Therefore, drastic shape changes cannot explain the observed behaviour. Further theoretical investigations should be pursued to understand this effect better, for example, on the configurations and reduced transition strengths for the associated states.

In the neighbouring nucleus  $^{62}\text{Ga}$ , the odd-spin yrast sequence has been observed to terminate at a spin-parity of  $17^+$ , and a backband is observed at the last transition [5]. These states can be envisioned to be built on a  $^{60}\text{Zn}$  core with a fully-aligned proton-neutron pair in the  $1g_{9/2}$  orbital, and the backband before the termination is therefore a reflection of the behaviour of the ground-state band in  $^{60}\text{Zn}$  [6]. However, a similar correspondence cannot be found in any other odd-odd  $N = Z$  nucleus in the region, as is evident from the comparisons in Fig. 10. In the figure, the bands built upon the  $J^\pi = 9^+$  states in the odd-odd  $N = Z$  nuclei with  $A = 58 - 74$  are compared to the ground-state bands of their respective core nuclei, which have one proton-neutron pair less. Yet, similarities between the other bands in the core nuclei can be found, for example, the similarity between the  $^{56}\text{Ni}$  [50,51] and  $^{58}\text{Cu}$  [41,49] bands built upon the proton-decaying states is striking. To investigate the relevance of this spectator model, which seems to work exceptionally well for  $^{62}\text{Ga}$ , requires comprehensive calculations for each relevant nucleus, but this is out of the scope of the current work.

An intriguing fact is, however, that similarity between the observed bands in  $^{66}\text{As}$  and those in its core  $^{64}\text{Ge}$ , with a proton-neutron pair removed, cannot be established with the current experimental knowledge. This could argue against

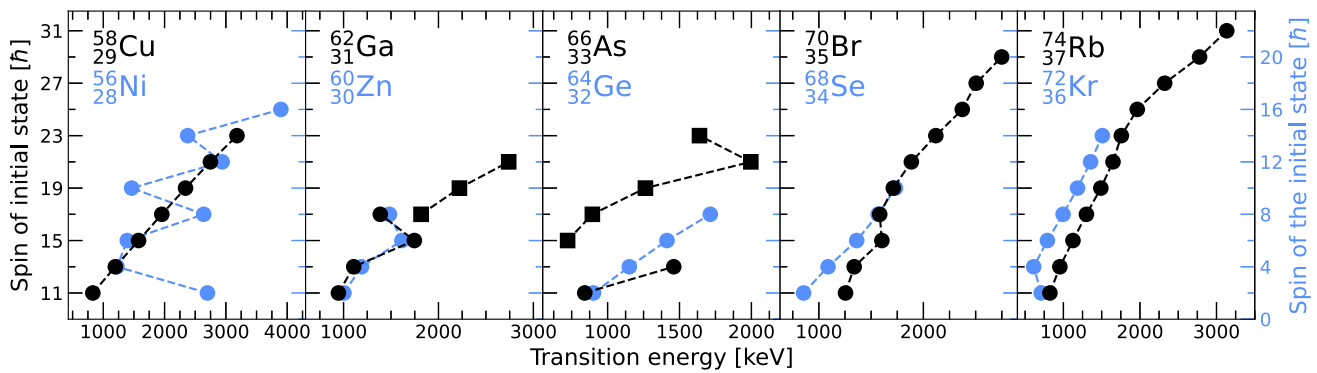


**Fig. 10** De-excitation paths along yrast odd-spin states down to the  $9^+$  state in the odd-odd  $N = Z$  nuclei between  $A = 58$ – $74$  and along the yrast even-spin states to the  $0^+$  ground state in their core nuclei. Data

on  $^{56}\text{Ni}$  [50,51],  $^{58}\text{Cu}$  [41,49],  $^{60}\text{Zn}$  [6],  $^{62}\text{Ga}$  [5],  $^{64}\text{Ge}$  [52],  $^{68}\text{Se}$  [53],  $^{70}\text{Br}$  [42],  $^{72}\text{Kr}$  [54], and  $^{74}\text{Rb}$  [48] are from the provided references

the picture of coupling an isoscalar  $np$  pair in the  $g_{9/2}$  orbital to the  $^{64}\text{Ge}$  core. It has been suggested that the addition of a fully aligned proton-neutron pair in a high- $j$  shell may flip the axis of rotation of a triaxial nucleus [55]. Such an occurrence is predicted also in  $^{66}\text{As}$  [7]: the addition of a fully-aligned  $T = 0$   $pn$  pair in the  $1g_{9/2}$  orbital to the triaxial  $^{64}\text{Ge}$  core switches the axis of rotation from the intermediate ( $\gamma \approx -30^\circ$ ) to the shortest ( $\gamma \approx +30^\circ$ ) axis. To experimentally investigate this scenario, the reduced transition probabilities and spectroscopic quadrupole moments, as calculated in Ref. [7], can prove to be useful, as they are sensitive to triaxiality and the rotational axis. The transition strengths can be accessed through measurement of the lifetimes of the states in the bands built upon the  $9^+$  isomeric state using the extremely clean conversion-electron tag utilised in this study.

## 5 Summary

The structure above the  $9^+$  isomeric state in  $^{66}\text{As}$  was studied in a fusion-evaporation reaction exploiting the conversion electrons emitted in the decay of the isomer. This conversion-electron tag eliminated contamination in the prompt  $\gamma$ -ray spectrum, which allowed us to establish the level ordering above the isomer using  $\gamma$ - $\gamma$  coincidences. Several new  $\gamma$ -ray transitions were observed, including those that have been identified before [20,21], but which were placed in the level scheme for the first time in the present work. The yrast band, which was previously assigned to have spins  $J^\pi = 12^+ - 16^+$ , has been reassigned to have odd-spin values starting from  $J = 13$  based on careful determination of angular distribution ratios, and it has been extended up to spin 23. The new results establish the spin assignments in  $^{66}\text{As}$  on a firmer footing. A comparison of the experimental states with the results of shell-model calculations using the  $jj44b$  and  $JUN45$  interactions suggest that the highest-energy yrast states are likely to have a positive parity. The role of the strong isoscalar  $pn$  pairing remains elusive.

The internal-conversion electrons from  $^{66}\text{As}$  allowed us to determine the true recoil- $\beta$  tagging efficiencies when using only the DSSD (22.7(3)%) and the DSSD+Tuiké [33] detectors (15.5(2)%) for the recoil-decay correlations. The latter value of 15.5(2)% does not include any specific energy requirement for the  $\beta$  particle detected in the scintillator, and the efficiency will reduce as the energy threshold is increased, as is commonly done when using the RBT method. This efficiency information is much needed when planning future  $\gamma$ -ray spectroscopy measurements around the  $N = Z$  line employing the  $\beta$ -tagging technique.

**Acknowledgements** The authors acknowledge the GAMMAPOOL European Spectroscopy Resource for the loan of the Germanium detectors. The authors would like to express their gratitude to the technical staff of the Accelerator Laboratory at the University of Jyväskylä (JYFL-ACCLAB) for their support.

**Author contributions** Data collection was performed by all JYFL-ACCLAB authors. Data analysis were performed by Henna Joukainen, Jan Sarén and Panu Ruotsalainen. Theoretical calculations were performed by Praveen C. Srivastava and Deepak Patel. The first draft of the manuscript was written by Henna Joukainen and all authors commented on previous versions of the manuscript. All authors read and approved the final manuscript.

**Funding** Open Access funding provided by University of Jyväskylä (JYU). Henna Joukainen has received funding for this study from the Vilho, Yrjö, and Kalle Väisälä foundation.

**Data availability** The experimental data for this article, and the corresponding metadata, are stored in the Finnish national FAIRdata repository and available from Ref. [56].

**Material Availability Statement** Not applicable to this work.

**Code availability** The codes used during analysis of the data are available from the corresponding author on reasonable request.

## Declarations

**Conflict of interest** The authors declare they have no Conflict of interest.

**Ethics approval and consent to participate** Not applicable to this work.

**Consent for publication** Not applicable to this work.

**Materials availability** Not applicable to this work.

**Open Access** This article is licensed under a Creative Commons Attribution 4.0 International License, which permits use, sharing, adaptation, distribution and reproduction in any medium or format, as long as you give appropriate credit to the original author(s) and the source, provide a link to the Creative Commons licence, and indicate if changes were made. The images or other third party material in this article are included in the article's Creative Commons licence, unless indicated otherwise in a credit line to the material. If material is not included in the article's Creative Commons licence and your intended use is not permitted by statutory regulation or exceeds the permitted use, you will need to obtain permission directly from the copyright holder. To view a copy of this licence, visit <http://creativecommons.org/licenses/by/4.0/>.

## References

1. S. Frauendorf, A.O. Macchiavelli, Overview of neutron–proton pairing. *Prog. Part. Nucl. Phys.* **78**, 24–90 (2014). <https://doi.org/10.1016/j.pnpnp.2014.07.001>
2. K. Kaneko, Y. Sun, G. de Angelis, Enhancement of high-spin collectivity in  $N=Z$  nuclei by the isoscalar neutron-proton pairing. *Nucl. Phys. A* **957**, 144–153 (2017). <https://doi.org/10.1016/j.nuclphysa.2016.08.007>
3. B. Cederwall, F.G. Moradi, T. Bäck, A. Johnson, J. Blomqvist, E. Clément, G. de France, R. Wadsworth, K. Andgren, K. Lagergren, A. Dijon, G. Jaworski, R. Liotta, C. Qi, B.M. Nyakó, J. Nyberg, M. Palacz, H. Al-Azri, A. Algora, G. de Angelis, A. Ataç, S. Bhat-tacharyya, T. Brock, J.R. Brown, P. Davies, A.D. Nitto, Z. Dombrádi, A. Gadea, J. Gál, B. Hadinia, F. Johnston-Theasby, P. Joshi, K. Juhász, R. Julin, A. Jungclaus, G. Kalinka, S.O. Kara, A. Khablanov, J. Kownacki, G.L. Rana, S.M. Lenzi, J. Molnár, R. Moro, D.R. Napoli, B.S.N. Singh, A. Persson, F. Recchia, M. Sandzelius, J.N. Scheurer, G. Sletten, D. Soehler, P.A. Söderström, M.J. Taylor, J. Timár, J.J. Valiente-Dobón, E. Vardaci, S. Williams, Evidence for a spin-aligned neutron-proton paired phase from the level structure of  $^{92}\text{Pd}$ . *Nature* **469**, 68–71 (2011). <https://doi.org/10.1038/nature09644>
4. H.M. David, P.J. Woods, G. Lotay, D. Seweryniak, M. Albers, M. Alcorta, M.P. Carpenter, C.J. Chiara, T. Davinson, D.T. Doherty, C.R. Hoffman, R.V.F. Janssens, T. Lauritsen, A.M. Rogers, S. Zhu, Low-lying  $T=0$  states in the odd-odd  $N=Z$  nucleus  $^{62}\text{Ga}$ . *Phys. Lett. B* **726**(4), 665–669 (2013). <https://doi.org/10.1016/j.physletb.2013.09.054>
5. D. Rudolph, I. Ragnarsson, S. Åberg, C. Andreoiu, M.P. Carpenter, R.M. Clark, J. Ekman, C. Fahlander, R.V.F. Janssens, F.G. Kondev, T. Lauritsen, D.G. Sarantites, D. Seweryniak, C.E. Svensson, Onset of high-spin rotational bands in the  $N = Z$  nucleus  $^{62}\text{Ga}$ . *Phys. Rev. C* **102**, 014313 (2020). <https://doi.org/10.1103/PhysRevC.102.014313>
6. C.E. Svensson, D. Rudolph, C. Baktash, M.A. Bentley, J.A. Cameron, M.P. Carpenter, M. Devlin, J. Eberth, S. Flibotte, A. Galindo-Uribarri, G. Hackman, D.S. Haslip, R.V.F. Janssens, D.R. LaFosse, T.J. Lampman, I.Y. Lee, F. Lerma, A.O. Macchiavelli, J.M. Nieminen, S.D. Paul, D.C. Radford, P. Reiter, L.L. Riedinger, D.G. Sarantites, B. Schaly, D. Seweryniak, O. Thelen, H.G. Thomas, J.C. Waddington, D. Ward, W. Weintraub, J.N. Wilson, C.H. Yu, A.V. Afanasjev, I. Ragnarsson, Decay out of the doubly magic superdeformed band in the  $N = Z$  nucleus  $^{60}\text{Zn}$ . *Phys. Rev. Lett.* **82**, 3400–3403 (1999). <https://doi.org/10.1103/PhysRevLett.82.3400>
7. P.C. Srivastava, S. Åberg, I. Ragnarsson, Triaxial rotation-axis flip triggered by an isoscalar  $np$  pair. *Phys. Rev. C* **95**, 011303(R) (2017). <https://doi.org/10.1103/PhysRevC.95.011303>
8. K.H. Schmidt, R.S. Simon, J.G. Keller, F.P. Hessberger, G. Münzenberg, B. Quint, H.G. Clerc, W. Schwab, U. Gollerthan, C.C. Sahn, Gamma-spectroscopic investigations in the radiative fusion reaction  $^{90}\text{Zr} + ^{90}\text{Zr}$ . *Phys. Lett. B* **168**(1), 39–42 (1986). [https://doi.org/10.1016/0370-2693\(86\)91456-5](https://doi.org/10.1016/0370-2693(86)91456-5)
9. R.S. Simon, K.H. Schmidt, F.P. Heßberger, S. Hlavac, M. Honusek, G. Münzenberg, H.G. Clerc, U. Gollerthan, W. Schwab, Evidence for nuclear shape coexistence in  $^{180}\text{Hg}$ . *Z. Phys. A* **325**(2), 197–202 (1986). <https://doi.org/10.1007/BF01289651>
10. E.S. Paul, P.J. Woods, T. Davinson, R.D. Page, P.J. Sellin, C.W. Beausang, R.M. Clark, R.A. Cunningham, S.A. Forbes, D.B. Fossan, A. Gizon, J. Gizon, K. Hauschild, I.M. Hibbert, A.N. James, D.R. LaFosse, I. Lazarus, H. Schnare, J. Simpson, R. Wadsworth, M.P. Waring, In-beam  $\gamma$ -ray spectroscopy above  $^{100}\text{Sn}$  using the new technique of recoil decay tagging. *Phys. Rev. C* **51**, 78–87 (1995). <https://doi.org/10.1103/PhysRevC.51.78>
11. D.M. Cullen, C. Scholey, C. Fox, A.J. Boston, E.S. Paul, H.C. Scraggs, S.L. Shepherd, O. Stezowski, T. Enqvist, P.A. Butler, A.M. Bruce, P.M. Walker, M. Caamaro, J. Garcés-Narro, M.A. Bentley, D.T. Joss, P.T. Greenlees, K. Helariutta, P.M. Jones, R. Julin, S. Juutinen, H. Kettunen, M. Leino, M. Muikku, O. Dorvaux, P. Rakhila, J. Uusitalo, P. Nieminen, Recoil-isomer tagging near the mass 140 proton drip line. *Nucl. Phys. A* **682**(1), 264–269 (2001). [https://doi.org/10.1016/S0375-9474\(00\)00649-7](https://doi.org/10.1016/S0375-9474(00)00649-7)
12. R. Julin, P.T. Greenlees, K. Helariutta, P. Jones, S. Juutinen, A.P. Leppänen, H. Kankaanpää, A. Keenan, H. Kettunen, P. Kuusiniemi, M. Leino, M. Muikku, P. Nieminen, J. Pakarinen, P. Rakhila, J. Uusitalo, D.T. Joss, S.J. Williams, D.G. Jenkins, N.S. Kelsall, R. Wadsworth, K. Hauschild, A. Hürstel, W. Korten, Y.L. Coz, A.N. Andreyev, P.V. Duppen, M. Huysse, K.V. de Vel, C.J. Moore, C.D. O'Leary, R.D. Page, M.J. Taylor, W. Reviol, M.B. Smith, In-beam studies of very neutron-deficient heavy nuclei. *Eur. Phys. J. A* **15**, 189–193 (2002). <https://doi.org/10.1140/epja/i2001-10252-6>
13. R. Julin, T. Grahn, J. Pakarinen, P. Rakhila, In-beam spectroscopic studies of shape coexistence and collectivity in the neutron-deficient  $Z \approx 82$  nuclei. *J. Phys. G* **43**(2), 024004 (2016). <https://doi.org/10.1088/0954-3899/43/2/024004>
14. K. Auranen, P. Siwach, P. Arumugam, A.D. Briscoe, L.S. Ferreira, T. Grahn, P.T. Greenlees, A. Herzán, A. Illana, D.T. Joss, H. Joukainen, R. Julin, H. Jutila, M. Leino, J. Louko, M. Luoma, E. Maglione, J. Ojala, R.D. Page, J. Pakarinen, P. Rakhila, J. Romero, P. Ruotsalainen, M. Sandzelius, J. Sarén, A. Tolosa-Delgado, J. Uusitalo, G. Zimba, Probing triaxiality beyond the proton drip line: Spectroscopy of  $^{147}\text{Tm}$ . *Phys. Rev. C* **108**, L011303 (2023). <https://doi.org/10.1103/PhysRevC.108.L011303>
15. A.N. Steer, D.G. Jenkins, R. Glover, B.S. Nara Singh, N.S. Pat-tabiraman, R. Wadsworth, S. Eeckhaudt, T. Grahn, P.T. Greenlees, P. Jones, R. Julin, S. Juutinen, M. Leino, M. Nyman, J. Pakarinen, P. Rakhila, J. Sarén, C. Scholey, J. Sorri, J. Uusitalo, P.A. Butler, I.G. Darby, R.D. Herzberg, D.T. Joss, R.D. Page, J. Thomson, R. Lemmon, J. Simpson, B. Blank, Recoil-beta tagging: A novel technique for studying proton-drip-line nuclei. *Nucl. Instrum. Methods Phys. Res. A* **565**(2), 630–636 (2006). <https://doi.org/10.1016/j.nima.2006.06.034>

16. J. Henderson, P. Ruotsalainen, D.G. Jenkins, C. Scholey, K. Auranen, P.J. Davies, T. Grahn, P.T. Greenlees, T.W. Henry, A. Herzañ, U. Jakobsson, P. Joshi, R. Julin, S. Juutinen, J. Konki, M. Leino, G. Lotay, A.J. Nichols, A. Obertelli, J. Pakarinen, J. Partanen, P. Peura, P. Rakkila, M. Sandzelius, J. Sarén, J. Sorri, S. Stolze, J. Uusitalo, R. Wadsworth, Enhancing the sensitivity of recoil-beta tagging. *J. Instrum.* **8**(4), P04025 (2013). <https://doi.org/10.1088/1748-0221/8/04/P04025>
17. D.M. Debenham, M.A. Bentley, P.J. Davies, T. Haylett, D.G. Jenkins, P. Joshi, L.F. Sinclair, R. Wadsworth, P. Ruotsalainen, J. Henderson, K. Kaneko, K. Auranen, H. Badran, T. Grahn, P. Greenlees, A. Herzañ, U. Jakobsson, J. Konki, R. Julin, S. Juutinen, M. Leino, J. Sorri, J. Pakarinen, P. Papadakis, P. Peura, J. Partanen, P. Rakkila, M. Sandzelius, J. Sarén, C. Scholey, S. Stolze, J. Uusitalo, H.M. David, G. de Angelis, W. Korten, G. Lotay, M. Mallaburn, E. Sahin, Spectroscopy of  $^{70}\text{Kr}$  and isospin symmetry in the  $T = 1$   $fp$ g shell nuclei. *Phys. Rev. C* **94**, 054311 (2016). <https://doi.org/10.1103/PhysRevC.94.054311>
18. X. Pereira-Lopez, M.A. Bentley, R. Wadsworth, P. Ruotsalainen, S.M. Lenzi, U. Forsberg, K. Auranen, A. Blazhev, B. Cederwall, T. Grahn, P. Greenlees, A. Illana, D.G. Jenkins, R. Julin, H. Jutila, S. Juutinen, X. Liu, R. Llewellyn, M. Luoma, K. Moschner, C. Müller-Gatermann, B.S.N. Singh, F. Nowacki, J. Ojala, J. Pakarinen, P. Papadakis, P. Rakkila, J. Romero, M. Sandzelius, J. Sarín, H. Tann, S. Uthayakumar, J. Uusitalo, G. Vega-Romero, J.M. Vilhena, R. Yajzey, W. Xhang, G. Zimba, In-beam  $\gamma$ -ray spectroscopy of  $^{94}\text{Ag}$ . *Eur. Phys. J. A* **59**(44) (2023). <https://doi.org/10.1140/epja/s10050-023-00950-8>
19. R. Grzywacz, S. Andriamonje, B. Blank, F. Boué, S. Czajkowski, F. Davi, R. Del Moral, C. Donzau, J.P. Dufour, A. Fleury, H. Grawe, A. Grewe, A. Heinz, Z. Janas, A.R. Junghans, M. Karny, M. Lewitowicz, A. Musquère, M. Pfützner, M.G. Porquet, M.S. Pravikoff, J.E. Sauvestre, K. Sümmerner, Isomeric states in  $^{66}\text{As}$ . *Phys. Lett. B* **429**(3), 247–253 (1998). [https://doi.org/10.1016/S0370-2693\(98\)00465-1](https://doi.org/10.1016/S0370-2693(98)00465-1)
20. R. Grzywacz, C. Yu, Z. Janas, S.D. Paul, J.C. Batchelder, C.R. Bingham, T.N. Ginter, C.J. Gross, J. McConnell, M. Lipoglavšek, A. Piechaczek, D.C. Radford, J.J. Ressler, K. Rykaczewski, J. Shergur, W. Walters, E.F. Zganjar, C. Baktash, M. Carpenter, R.V.F. Janssens, C.E. Svensson, J.C. Waddington, D. Ward, E. Dragulescu, In-beam study of the  $N=Z$  nucleus  $^{66}_{33}\text{As}_{33}$  using the decay tagging technique. *Nucl. Phys. A* **682**(1), 41c–47c (2001). [https://doi.org/10.1016/S0375-9474\(00\)00620-5](https://doi.org/10.1016/S0375-9474(00)00620-5)
21. P. Ruotsalainen, C. Scholey, R. Julin, K. Hauschild, K. Kaneko, B.S. Nara Singh, R. Wadsworth, D.G. Jenkins, T.S. Brock, P.T. Greenlees, J. Henderson, U. Jakobsson, P. Jones, S. Juutinen, S. Ketelhut, M. Leino, N.M. Lumley, P.J.R. Mason, P. Nieminen, M. Nyman, I. Paterson, P. Peura, M.G. Procter, P. Rakkila, J. Sarén, J. Sorri, J. Uusitalo, Recoil- $\beta$  tagging study of the  $N = Z$  nucleus  $^{66}\text{As}$ . *Phys. Rev. C* **88**, 024320 (2013). <https://doi.org/10.1103/PhysRevC.88.024320>
22. A. Petrovici, K.W. Schmid, A. Faessler, Neutron-proton pairing correlations in medium mass  $N \approx Z$  nuclei. *Nucl. Phys. A* **647**(3), 197–216 (1999). [https://doi.org/10.1016/S0375-9474\(99\)00004-4](https://doi.org/10.1016/S0375-9474(99)00004-4)
23. G. de Angelis, K.T. Wiedemann, T. Martinez, R. Orlandi, A. Petrovici, E. Sahin, J.J. Valiente-Dobón, D. Tonev, S. Lunardi, B.S. Nara Singh, R. Wadsworth, A. Gadea, K. Kaneko, P.G. Bizzetti, A.M. Bizzetti-Sona, B. Blank, A. Bracco, M.P. Carpenter, C.J. Chiara, E. Farnea, A. Gottardo, J.P. Greene, S.M. Lenzi, S. Leoni, C.J. Lister, D. Mengoni, D.R. Napoli, O.L. Pechenaya, F. Recchia, W. Reviol, D.G. Sarantites, D. Seweryniak, C.A. Ur. S. Zhu, Shape isomerism and shape coexistence effects on the Coulomb energy differences in the  $N = Z$  nucleus  $^{66}\text{As}$  and neighboring  $T = 1$  multiplets. *Phys. Rev. C* **85**, 034320 (2012). <https://doi.org/10.1103/PhysRevC.85.034320>
24. O. Juillet, P. Van Isacker, D.D. Warner, Interacting boson model for exotic nuclei at low isospin. *Phys. Rev. C* **63**, 054312 (2001). <https://doi.org/10.1103/PhysRevC.63.054312>
25. P.V. Isacker, O. Juillet, Symmetry in exotic nuclei. *Eur. Phys. J. A* **15**, 233–236 (2002). <https://doi.org/10.1140/epja/i2001-10260-6>
26. E. Baldini-Neto, C.L. Lima, P. Van Isacker, Binding energies of  $T = 0$  and  $T = 1$  ground states of  $N = Z$  nuclei in the interacting boson model. *Phys. Rev. C* **65**, 064303 (2002). <https://doi.org/10.1103/PhysRevC.65.064303>
27. R. Sahu, V.K.B. Kota, Deformed shell model for  $T = 0$  and  $T = 1$  bands in  $^{62}\text{Ga}$  and  $^{66}\text{As}$ . *Phys. Rev. C* **66**, 024301 (2002). <https://doi.org/10.1103/PhysRevC.66.024301>
28. M. Hasegawa, Y. Sun, K. Kaneko, T. Mizusaki, Structure of isomeric states in  $^{66}\text{As}$  and  $^{67}\text{As}$ . *Phys. Lett. B* **617**(3), 150–156 (2005). <https://doi.org/10.1016/j.physletb.2005.05.027>
29. M. Honma, T. Otsuka, T. Mizusaki, M. Hjorth-Jensen, New effective interaction for  $f_5p$ g $_9$ -shell nuclei. *Phys. Rev. C* **80**, 064323 (2009). <https://doi.org/10.1103/PhysRevC.80.064323>
30. P.C. Srivastava, R. Sahu, V.K.B. Kota, Shell model results for  $T = 1$  and  $T = 0$  bands in  $^{66}\text{As}$ . *J. Phys. G* **44**(12), 125107 (2017). <https://doi.org/10.1088/1361-6471/aa946d>
31. B.A. Brown, A.F. Lisetskiy, Unpublished
32. B. Cheal, E. Mané, J. Billowes, M.L. Bissell, K. Blaum, B.A. Brown, F.C. Charlwood, K.T. Flanagan, D.H. Forest, C. Geppert, M. Honma, A. Jokinen, M. Kowalska, A. Krieger, J. Krämer, I.D. Moore, R. Neugart, G. Neyens, W. Nörtershäuser, M. Schug, H.H. Stroke, P. Vingerhoets, D.T. Yordanov, M. Žáková, Nuclear spins and moments of Ga isotopes reveal sudden structural changes between  $N = 40$  and  $N = 50$ . *Phys. Rev. Lett.* **104**, 252502 (2010). <https://doi.org/10.1103/PhysRevLett.104.252502>
33. H. Joukainen, J. Sarén, P. Ruotsalainen, Position sensitive plastic scintillator for beta particle detection. *Nucl. Instr. Methods Phys. Res. A* **1027**, 166253 (2022). <https://doi.org/10.1016/j.nima.2021.166253>
34. J. Uusitalo, J. Sarén, J. Partanen, J. Hilton, Mass analyzing recoil apparatus. *MARA. Acta Phys. Pol. B* **50**(3), 319–327 (2019). <https://doi.org/10.5506/APhysPolB.50.319>
35. J. Sarén, J. Uusitalo, H. Joukainen, In-flight recoil separators RITU and MARA and the standard detector setups. *Nucl. Instrum. Methods Phys. Res. B* **541**, 33–36 (2023). <https://doi.org/10.1016/j.nimb.2023.04.040>
36. J. Pakarinen, J. Ojala, P. Ruotsalainen, H. Tann, H. Badran, T. Calverley, J. Hilton, T. Grahn, P.T. Greenlees, M. Hytönen, A. Illana, A. Kauppinen, M. Luoma, P. Papadakis, J. Partanen, K. Porras, M. Puskala, P. Rakkila, K. Ranttila, J. Sarén, M. Sandzelius, S. Szvec, J. Tuunanen, J. Uusitalo, G. Zimba, The JROGAM 3 spectrometer. *Eur. Phys. J. A* **56**, 149 (2020). <https://doi.org/10.1140/epja/s10050-020-00144-6>
37. J. Ziegler. SRIM—the stopping and range of ions in matter. <http://www.srim.org/>. TRIM version 2013 used. Accessed 15 Jan 2024
38. J.P. Biersack, L.G. Hagmark, A Monte Carlo computer program for the transport of energetic ions in amorphous targets. *Nucl. Instrum. Methods* **174**, 257–269 (1980). [https://doi.org/10.1016/0029-554X\(80\)90440-1](https://doi.org/10.1016/0029-554X(80)90440-1)
39. E. Browne, J.K. Tuli, Nuclear data sheets for  $A = 66$ . *Nucl. Data Sheets* **111**(4), 1093–1209 (2010). <https://doi.org/10.1016/j.nds.2010.03.004>
40. M. Wang, W.J. Huang, F.G. Kondev, G. Audi, S. Naimi, The AME 2020 atomic mass evaluation (II). tables, graphs and references\*. *Chin. Phys. C* **45**(3), 030003 (2021). <https://doi.org/10.1088/1674-1137/abddaf>
41. D. Rudolph, D.G. Sarantites, C. Andreou, C. Fahlander, D.P. Balamuth, R.J. Charity, M. Devlin, J. Eberth, A. Galindo-Uribarri, P.A. Hausladen, D. Seweryniak, L.G. Sobotka, T. Steinhardt, High-resolution in-beam particle spectroscopy -new results on prompt



- proton emission from  $^{58}\text{Cu}$ . *Eur. Phys. J. A* **14**, 137–146 (2002). <https://doi.org/10.1140/epja/i2002-10005-1>
42. D.G. Jenkins, N.S. Kelsall, C.J. Lister, D.P. Balamuth, M.P. Carpenter, T.A. Sienko, S.M. Fischer, R.M. Clark, P. Fallon, A. Görgen, A.O. Macchiavelli, C.E. Svensson, R. Wadsworth, W. Reviol, D.G. Sarantites, G.C. Ball, J. Rikowska Stone, O. Juillet, P. Van Isacker, A.V. Afanasjev, S. Frauendorf,  $T = 0$  and  $T = 1$  states in the odd-odd  $N = Z$  nucleus,  $^{70}_{35}\text{Br}_{35}$ . *Phys. Rev. C* **65**, 064307 (2002). <https://doi.org/10.1103/PhysRevC.65.064307>
  43. P. Müller, S. Kaufmann, T. Miyagi, J. Billowes, M.L. Bissell, K. Blaum, B. Cheal, R.F. Garcia Ruiz, W. Gins, C. Gorges, H. Heylen, A. Kanellakopoulos, S. Malbrunot-Ettenauer, R. Neugart, G. Neyens, W. Nörtershäuser, T. Ratajczyk, L.V. Rodríguez, R. Sánchez, S. Sailer, A. Schwenk, L. Wehner, C. Wraith, L. Xie, Z.Y. Xu, X.F. Yang, D.T. Yordanov, Electromagnetic moments of the odd-mass nickel isotopes  $^{59-67}\text{Ni}$ . *Phys. Lett. B* **854**, 138737 (2024). <https://doi.org/10.1016/j.physletb.2024.138737>
  44. U. Silwal, J.A. Winger, S.V. Ilyushkin, K.P. Rykaczewski, C.J. Gross, J.C. Batchelder, L. Cartegni, I.G. Darby, R. Grzywacz, A. Korgul, W. Królas, S.N. Liddick, C. Mazzocchi, A.J. Mendez, S. Padgett, M.M. Rajabali, D.P. Siwakoti, D. Shapira, D.W. Stracener, E.F. Zganjar,  $\beta$  decay of neutron-rich  $^{76}\text{Cu}$  and the structure of  $^{76}\text{Zn}$ . *Phys. Rev. C* **106**, 044311 (2022). <https://doi.org/10.1103/PhysRevC.106.044311>
  45. V. Kumar, A. Kumar, P.C. Srivastava, Shell-model study for gt-strengths corresponding to  $\beta$  decay of  $^{60}\text{Ge}$  and  $^{62}\text{Ge}$ . *Nucl. Phys. A* **1017**, 122344 (2022). <https://doi.org/10.1016/j.nuclphysa.2021.122344>
  46. D. Patel, P.C. Srivastava, V.K.B. Kota, R. Sahu, Large-scale shell-model study of two-neutrino double beta decay of  $^{82}\text{Se}$ ,  $^{94}\text{Zr}$ ,  $^{108}\text{Cd}$ ,  $^{124}\text{Sn}$ ,  $^{128}\text{Te}$ ,  $^{130}\text{Te}$ ,  $^{136}\text{Xe}$ , and  $^{150}\text{Nd}$ . *Nucl. Phys. A* **1042**, 122808 (2024). <https://doi.org/10.1016/j.nuclphysa.2023.122808>
  47. N. Shimizu, T. Mizusaki, Y. Utsuno, Y. Tsunoda, Thick-restart block Lanczos method for large-scale shell-model calculations. *Comput. Phys. Commun.* **244**, 372–384 (2019). <https://doi.org/10.1016/j.cpc.2019.06.011>
  48. C.D. O’Leary, C.E. Svensson, S.G. Frauendorf, A.V. Afanasjev, D.E. Appelbe, R.A.E. Austin, G.C. Ball, J.A. Cameron, R.M. Clark, M. Cromaz, P. Fallon, D.F. Hodgson, N.S. Kelsall, A.O. Macchiavelli, I. Ragnarsson, D. Sarantites, J.C. Waddington, R. Wadsworth, Evidence for isovector neutron-proton pairing from high-spin states in  $N = Z$   $^{74}\text{Rb}$ . *Phys. Rev. C* **67**, 021301(R) (2003). <https://doi.org/10.1103/PhysRevC.67.021301>
  49. D. Rudolph, C. Baktash, J. Dobaczewski, W. Nazarewicz, W. Satuła, M.J. Brinkman, M. Devlin, H.Q. Jin, D.R. LaFosse, L.L. Riedinger, D.G. Sarantites, C.H. Yu, Prompt proton decay of a well-deformed rotational band in  $^{58}\text{Cu}$ . *Phys. Rev. Lett.* **80**, 3018–3021 (1998). <https://doi.org/10.1103/PhysRevLett.80.3018>
  50. D. Rudolph, C. Baktash, M.J. Brinkman, E. Caurier, D.J. Dean, M. Devlin, J. Dobaczewski, P.H. Heenen, H.Q. Jin, D.R. LaFosse, W. Nazarewicz, F. Nowacki, A. Poves, L.L. Riedinger, D.G. Sarantites, W. Satuła, C.H. Yu, Rotational bands in the doubly magic nucleus  $^{56}\text{Ni}$ . *Phys. Rev. Lett.* **82**, 3763–3766 (1999). <https://doi.org/10.1103/PhysRevLett.82.3763>
  51. E.K. Johansson, D. Rudolph, L.L. Andersson, D.A. Torres, I. Ragnarsson, C. Andreoiu, C. Baktash, M.P. Carpenter, R.J. Charity, C.J. Chiara, J. Ekman, C. Fahlander, C. Hoel, O.L. Pechenaya, W. Reviol, R. du Rietz, D.G. Sarantites, D. Seweryniak, L.G. Sobotka, C.H. Yu, S. Zhu, Prompt proton decay and deformed bands in  $^{56}\text{Ni}$ . *Phys. Rev. C* **77**, 064316 (2008). <https://doi.org/10.1103/PhysRevC.77.064316>
  52. P.J. Ennis, C.J. Lister, W. Gelletly, H.G. Price, B.J. Varley, P.A. Butler, T. Hoare, S. Ćwiok, W. Nazarewicz, Triaxiality and isospin-forbidden E1 decays in the  $N = Z$  nucleus  $^{64}\text{Ge}$ . *Nucl. Phys. A* **535**(2), 392–424 (1991). [https://doi.org/10.1016/0375-9474\(91\)90454-E](https://doi.org/10.1016/0375-9474(91)90454-E)
  53. S.M. Fischer, D.P. Balamuth, P.A. Hausladen, C.J. Lister, M.P. Carpenter, D. Seweryniak, J. Schwartz, Evidence for collective oblate rotation in  $N = Z$   $^{68}\text{Se}$ . *Phys. Rev. Lett.* **84**, 4064–4067 (2000). <https://doi.org/10.1103/PhysRevLett.84.4064>
  54. N.S. Kelsall, R. Wadsworth, A.N. Wilson, P. Fallon, A.O. Macchiavelli, R.M. Clark, D.G. Sarantites, D. Seweryniak, C.E. Svensson, S.M. Vincent, S. Frauendorf, J.A. Sheikh, G.C. Ball, Consequences of neutron-proton pairing correlations for the rotational motion of the  $N = Z$  nucleus  $^{72}\text{Kr}$ . *Phys. Rev. C* **64**, 024309 (2001). <https://doi.org/10.1103/PhysRevC.64.024309>
  55. A. Juodagalvis, S. Åberg, Rotational structure of  $T = 0$  and  $T = 1$  bands in the  $N = Z$  nucleus  $^{62}\text{Ga}$ . *Nucl. Phys. A* **683**(1), 207–226 (2001). [https://doi.org/10.1016/S0375-9474\(00\)00441-3](https://doi.org/10.1016/S0375-9474(00)00441-3)
  56. P. Ruotsalainen, H. Joukainen, J. Saren, J. Uusitalo, K. Auranen, T. Grahn, P. Greenlees, R. Julin, H. Jutila, J. Pakarinen, P. Rähkila, A.I. Sison, M. Luoma, J. Louko, J. Ojala, M. Sandzelius, H. Tann, G. Zimba, Z. Ge. JYFL – ACCLAB – JM22: Towards understanding of isospin-breaking effects in isobaric multiplets: In-beam recoil-beta tagging study of  $^{66}\text{Se}$  and  $^{66}\text{As}$  (2024). <https://doi.org/10.23729/38892b63-c85b-48ff-9ff7-9d3ec423b7e1>